Mon. Not. R. Astron. Soc. **000**, 000–000 (0000) Printed 11 October 1999 (MN LaTeX style file v1.3)

Luminous and Dark Matter in the Milky Way

Rob P. Olling[A,B,⋆], Michael R. Merrifield[B,†]

[A] *Dept. of Physics and Astronomy, Rutgers University, P.O. Box 849, Piscataway, NJ 08855-0849, U.S.A.*
[B] *School of Physics and Astronomy, University of Nottingham, University Park, Nottingham, NG7 2RD*

11 October 1999

ABSTRACT

Strong interrelations exist between the Galactic constants [the Sun's distance to the Galactic centre (R_0), and the local rotation speed (Θ_0)], the stellar columndensity (Σ_*) and the shortest-to-longest axis ratio of the dark matter halo (q). In this paper we present simple analytical approximations that allow for an efficient search through the vastness of parameter space, and apply this approximation to investigate the consequences of the uncertain gaseous velocity dispersion (σ_g) on the constraints imposed by the thickness of the Milky Way's gas layer. The extra degree of freedom does not significantly alter the conclusions drawn in a previous paper regarding the shape of the Milky Way's dark matter halo. A significant contribution to the total gas pressure by cosmic rays and magnetic fields beyond the optical disk is thus ruled out. We find that the Milky Way's dark halo is close to spherical if $R_0 \gtrsim 7.1$ kpc, while a significantly flattened dark matter halo is only possible if our distance to the Galactic centre is smaller than ~ 6.8 kpc.

It is only possible to construct a self-consistent model of the Galaxy based on the IAU-recommended values for the Galactic constants ($R_0 = 8.5$ kpc, $\Theta_0 = 220$ km s^{-1}) if the effective gaseous velocity dispersion is ~17% larger than observed, *and* if the local stellar columndensity is less than about 22 $M_\odot$ pc^{-2}. If we assume that the halo is oblate, that non-thermal pressure support of the gas layer is minimal and a value of Σ_* of 35 ± 5 $M_\odot$ pc^{-2}(Kuijken & Gilmore 1989b), we can rule out Galactic models with $R_0 \gtrsim 8.0$ kpc or $\Theta_0 \gtrsim 200$ km s^{-1}., whatever the value of σ'_g.

By analyzing the vertical force law in a self-consistent Galaxy model, we have uncovered a "vertical disk-halo conspiracy," which formalizes the well known fact that stellar kinematical data alone are insufficient to determine the columndensity of stars in the Solar neighbourhood. Combining the best kinematical and star-count estimates of Σ_*, we suggest that a value of Σ_*= 35 ± 10 $M_\odot$ pc^{-2} is an appropriate consensus average. We find that Kuijken & Gilmore's (1991) determination of the columndensity of matter within 1.1 kpc of the plane is robust and valid over a wide range of Galactic constants.

Our mass models show that, largely due to the uncertainty in the Galactic light distribution, the dark matter density in the Galactic centre is uncertain by up to three orders of magnitude. In the Solar neighbourhood this uncertainty is much reduced: our models imply a dark matter density of some 0.42 GeV/c^2 per cubic centimetre, or (11 ± 5) m$M_\odot$ pc^{-3}– roughly 15% of the total mass density.

Key words: Galaxy: structure - Galaxy: kinematics and dynamics - Galaxy: solar neighborhood - Galaxy: fundamental parameters - Galaxy: stellar content

⋆ E-mail: olling@astro.rutgers.edu
† E-mail: Michael.Merrifield@Nottingham.ac.uk

1 INTRODUCTION

The observational fact that rotation curves of external galaxies are rather flat in their outer parts (Rubin, Ford & Thonnard 1980; Bosma 1981; Kent 1987; Begeman 1987; Casertano & van Gorkom 1991; Broeils 1992; Persic, Salucci & Stel 1996) indicates the presence of unseen matter in those galaxies[‡]. A problem which is specific for the Milky Way is that we do not know the shape of the Galactic rotation curve. The slope depends on the assumed values of the Galactic constants (Olling & Merrifield 1998). But dark matter is required whatever the values of the Galactic constants. A fit to the observed rotation curve can be used to yield the stellar mass-to-light ratio $\Upsilon_{\rm d}$, and the dark halo parameters, albeit with large uncertainties. Rather than using this fitting procedure, we adopt an analytical approximation in which there is only one free parameter: the degree to which the disk is maximal (γ), from which $\Upsilon_{\rm d}$ and the dark halo parameters follow (see Olling 1995 for details). The parameter γ is preferred for dynamical modeling purposes as it is bound between 0 and 1, zero mass and a full-fledged disk, respectively. For example, in the popular "maximum-disk" hypothesis (van Albada & Sancisi 1986), the amplitude of the stellar rotation curve equals (85 ± 10)% of the observed rotation speed (Sackett 1997), so that $\gamma = 0.85$. In contrast, Bottema (1993) used stellar velocity dispersion measurements to "weigh" stellar disks, and concluded that they are sub-maximal, with $\gamma = 0.63 \pm 0.1$. The situation is similarly indeterminate for the Milky Way: the Kuijken & Gilmore (1989, hereafter referred to as KG89) model implies $\gamma \sim 0.5$, while more recent models with lower rotation speed and shorter scale-lengths can be close to maximal ($\gamma = 0.85 \pm 0.1$; Sackett 1997). As a result of the uncertain stellar mass-to-light ratio, the dark halo parameters are very ill determined for most galaxies (e.g., van Albada & Sancisi 1986; Lake & Feinswog 1989; Olling 1995). The Milky Way is no different: the combined uncertainty in the local disk mass and the stellar scale-length introduces an uncertainty of over three orders of magnitude in the central dark matter (DM) density of the Milky Way, and about an order of magnitude uncertainty in its core radius (§2;Dehnen & Binney 1998). In the Solar neighborhood the situation is less dramatic, although no consensus exists on the local volume density of dark matter [ρ_{DM} or the Oort limit; see §2 and Crézé *et al.* (1998) for a recent review]. However, the local dark matter density is important for many astrophysical problems. For example, if the dark matter comprises elementary particles like neutralinos, axions, neutrinos, gravitinos etc., their expected detection rate is proportional to the DM density. Likewise, if the dark halo is made up of massive compact halo objects (MACHOs), the event rate for gravitational lensing depends on the integrated dark matter density along the line of sight towards the lens. Thus, observational signatures of the Milky Way's dark matter distribution like micro-lensing time scales and optical depths (Gates, Gyuk & Turner 1995), and expected neutralino annihilation rate (Bergstrom, Ullio & Buckley 1997) depend on the Galactic dark matter density distribution and hence the assumed values for the Galactic constants.

In a previous paper (Olling & Merrifield 1999, henceforth Paper I) we determined the dark matter density in the Solar neighbourhood at $R = R_0$[§] and around $R \sim 2R_0$ to infer the minor to major axial ratio ($q = c/a$), or shape, of the dark matter halo of the Milky Way. In the present paper we investigate the reliability of several of the assumptions made in Paper I, and find that relaxing these assumptions does not greatly change the conclusion of Paper I: the shape of the dark matter halo of the Milky Way is probably rather round. Before going into more detail, let us review some of the difficulties which arise when one tries to determine ρ_{DM}.

First, large values of the local Galactic rotation speed (Θ_0) result in large DM densities, while low rotation speeds require small DM densities. Second, since the *shape* of the Galactic rotation curve depends on the value of our distance to the Galactic center (Olling & Merrifield 1998), the amount of dark matter increases with R_0 at constant Θ_0. And finally, more highly flattened DM halos have larger midplane densities (Olling 1995).

We use two sets of observations to constrain the midplane dark matter density. First, stellar kinematical data provides a measure of the total columndensity within 1.1 kpc of the plane (Kuijken & Gilmore 1991). The dark matter density follows after subtracting the luminous component and dividing by the scale-height. This method yield ambiguous results because uncertainties in the surface density of stellar matter (Σ_*) translate into a similar uncertainty of the DM density. Thus, low values of Σ_* require more highly flattened dark halos at constant (R_0,Θ_0).

Second, the rate at which the thickness of the gas layer increases with radius ("flaring") is a measure of ρ_{DM}. Assuming, for now, a hydrostatic balance between internal pressure and gravity, it follows that an increasing gas layer width is evidence for a decreasing midplane density. Large dark matter densities result in thin gas layers, while low densities yield a thicker gas disk. A larger DM density, due to either a larger Θ_0 and/or R_0 or a smaller q, results in a thinner gas layer. However, such a thinner gas layer would also occur if the actual gas pressure –or equivalently, the gaseous velocity dispersion, σ_g– is smaller than assumed. Hence the significant correlations between the assumed values of the Galactic constants, Σ_* and σ_g and the inferred shape of the Milky Way's dark matter halo referred to above.

In practice, the stellar kinematical data impose correlations between Θ_0 and q at the Solar circle, while the observed H I flaring does so at $R \sim (2 \pm 0.25)R_0$. At these large radii the stellar disk has disappeared so that the potential is dominated by the gaseous self-gravity and the dark matter.

‡ See McGaugh & de Blok (1998) for a review of the alternative hypothesis that the law of gravity has to be modified instead.

§ Throughout this paper we use cylindrical coordinates with R the Galactocentric distance, and z the distance of the plane.

Unfortunately, the Galactic constants are ill-determined (Kerr & Lynden-Bell 1986; Reid 1993; Paper I), and this has consequences for analyses which depend on R_0 and Θ_0. In an ideal world, parameters such as the Galactic constants, the rotation curve [$\Theta(R)$], the scale-length of the optical disk ($h_{\rm d}$), the local stellar column density, the gaseous velocity dispersion, the halo's shape, and so forth, are not only measured, but also have normal errors. In that case one could determine quantities that depend on these parameters, such as the DM density or the halo's shape, by comparing the model and observed parameters in a χ^2 sense. Unfortunately, the quoted errors on R_0 and Θ_0 are not normal, and the values themselves are not averages in the statistical sense, but are rather *consensus* values with consensus errors. These arguments lead to the conclusion that the *values* of the Galactic constants and their errors *can not* be used in analyses like maximum-likelihood estimates of a property X which depends on the Galactic constants. Instead we urge researchers to investigate the dependence of their results on the assumed values of the Galactic constants and present their conclusions as functions of R_0 and Θ_0. Given the tremendous increase in computing power, such an approach may currently be more feasible than in the past. Practicing what we preach, we follow this approach in previous papers (Olling & Merrifield 1998,1999) as well as in the current article.

In Paper I we used both the constraints set by the flaring of the H I layer as well as the boundary conditions imposed by the local stellar kinematics to infer the halo's flattening. The procedure works as follows: 1) pick values for R_0 and Θ_0 and determine the corresponding rotation curve, 2) create mass models with as ingredients the stellar disk, the interstellar medium (ISM) and a dark halo of varying degrees of flattening, 3) pick values for the scale-length and mass of the stellar disk, 4) select a value for σ_g and calculate model flaring curves (Olling 1995), 5) select the model with flattening q such that the observed H I flaring at $R \sim 2R_0$ is reproduced [this flattening will be independent of the distribution of the stellar mass (Olling 1995)], 6) vary Σ_* and $h_{\rm d}$ till the model columndensity within 1.1 kpc of the plane agrees with the observed value. In this manner we construct self-consistent mass models, with specific values for $h_{\rm d}$, Σ_* and q, for any combination of the Galactic constants. Possibly the weakest link in this procedure is the assumed value for σ_g. In the present paper we will remedy this shortcoming of Paper I by repeating the procedure outlined above for many values of the gaseous velocity dispersion. Picking a value for σ_g in the outer Galaxy is related to the question as to the relevance of non-thermal pressure support (due to magnetic fields and cosmic rays) of the gas layer. We investigate these issues in detail in section 4.

The surface density of stars in the Solar neighbourhood provides a significant constraint on the determination of the halo's shape. We therefore review recent determinations in section 3.1. Kuijken & Gilmore (1991, henceforth KG91) claim that the columndensity within 1.1 kpc of the plane is much better determined than the values of the individual components. However, their Galactic constants lie at the high end of the range we use. Since $\Sigma_{tot}^{1.1}$ provides us with such an important constraint, we consider it prudent to check KG91's assertion. We indeed confirm KG91's claim that $\Sigma_{tot}^{1.1}$ is relatively well determined over a large range in Galactic constants, Σ_* and $h_{\rm d}$ (Appendix A). In the following section we describe our mass models in more detail and determine the density of dark matter in the Solar neighbourhood. We summarize and conclude in §5.

2 MASS MODELS

In order to interpret the available data we build Milky Way mass models for which we determine the model values of the total disk mass, the H I flaring, and other parameters. A comparison between the observations and the models yields the size, mass and shape of the Milky Way. Our models include: a stellar bulge and disk, a gas layer, and a dark halo. Some of the relevant parameters of our models are tabulated in Table 1. We consider models with a range of Galactic constants, disk exponential scale-length, stellar disk mass, total columndensity, and halo flattening. To calculate the *exact* vertical force law ($K_{\rm z}(R,z)$) at every point (R,z)¶ in the Galaxy we integrate over the full mass distribution: $K_{\rm z}(R,z) = G \int_0^\infty r dr \rho(r,0) \int_{-\infty}^\infty dw \rho(r,w) \int_{-\pi}^{\pi} \frac{d}{dz} \frac{d\theta}{|\overline{\rm s} - \overline{\rm S}|}$ with $\overline{\rm s} = \{r, w\}, \overline{\rm S} = \{R, z\}$, ρ the total mass density at (R,z), and G Newton's constant of gravity (Olling 1995). Since the calculation of $K_{\rm z}$ and the model flaring curve is rather expensive‖ we perform these detailed calculations only for the limited subset of models listed in Table 2. We determine the model flaring curves for a much larger range in R_0 and Θ_0 values by applying an approximation (Olling 1995, Appendix D) which we calibrate using the models presented in Table 2, see section 3.3 for further details.

2.1 The Mass Components

We base our model for the bulge on Kent's (1992) K-band luminosity distribution. The bulge is a modified spheroid with "boxy" appearance and density: $\rho_b(s) = d_b\ K_0(s/h_b)$, with $s^4 = R^4 + (z/q_b)^4 + \zeta_b^4$. The bulge is flattened with axial ratio q_b. To avoid the singularity of the K_0-Bessel function at $s = 0$, we include a softening ζ_b. We also truncate the bulge exponentially beyond 3 kpc.

For the disk, we use the standard form of a radially exponential disk with central surface brightness $L_{\rm d,K}(0)$ and scale-length $h_{\rm d}$. We will consider models with values for the scale-length which are considered to be reasonable (Sackett 1997). Furthermore we use the observational fact that the total luminosity is better determined than either the central surface brightness or the scale-length (Kent, Dame & Fazio 1991). Thus, we scale $L_{\rm d,K}(0)$ such that the total luminosity is conserved for each choice of $h_{\rm d}$. However, the numerical values of $L_{\rm d,K}(0)$ and $h_{\rm d}$ depend on our choice

¶ We assume azimuthal symmetry.

‖ The calculation of model gas layer widths for a given combination of R_0, Θ_0, $h_{\rm d}$ and bulge and disk mass-to-light ratios takes about 1.3 hours per q-values, on a 50 MHz dual processor SPARC-10.

Table 1. Some parameters used in the model calculations.

bulge:		
d_b	3.53	$L_{\odot,K}$ pc^{-3}
q_b	0.61	
h_b	667	pc
ζ_b	10	pc
$\rho_b(0)$	15.24	$L_{\odot,K}$ pc^{-3}
$L_{b,K,tot}$	1.5 10^{10}	$L_{\odot,K}$
disk:		
z_e	300	pc
h_d	2, 2.5, 3	kpc
$L_{\rm d,K}(0)$	2200, 1408, 978	$L_{\odot,K}$ pc^{-2} ($h_{\rm d}$=2,2.5,3)
$\Sigma_*(R_0)$	25-45	$L_\odot$ pc^{-2}
ρ_*	26.5 - 47.7	10^{-3} $M_\odot$ pc^{-3}
$L_{d,K,tot}$	5.5 10^{10}	$L_{\odot,K}$
ISM at R_0:		
$\Sigma_{\rm H\ I\ +H\ II}$	9.25	$M_\odot$ pc^{-2}
$\Sigma_{\rm H_2}$	1.80	$M_\odot$ pc^{-2}
FWHM$_{\rm H\ I}$	410 ± 30	$(R_0/7.1)$ pc
FWHM$_{\rm H_2}$	141 ± 20	$(R_0/7.1)$ pc
$\rho_{\rm H\ I\ +H\ II}$	21 ± 1.5	$(7.1/R_0)$ 10^{-3} $M_\odot$ pc^{-3}
$\rho_{\rm H_2}$	12 ± 1.5	$(7.1/R_0)$ 10^{-3} $M_\odot$ pc^{-3}
ρ_{ISM}	43 ± 3.0	$(7.1/R_0)$ 10^{-3} $M_\odot$ pc^{-3}

of R_0. From Freudenreich (1996, 1998) we find that these quantities typically increase with R_0, by 8%× (R_0/kpc - 8). Such variations induce a change in total luminosity which is a factor of three larger. However, because these corrections are smaller than the changes resulting from the uncertainty in $h_{\rm d}$, we do not scale $L_{d,K,tot}$ with R_0. For the disk's vertical distribution we use a secant-hyperbolic function [sech($\frac{z}{2*z_e}$)], which is a compromise between the often used exponential and secant-hyperbolic-squared forms (van der Kruit 1988). For simplicity, the exponential scale-height ($z_{\rm e}$) of the disk is taken to be constant at 300 pc, intermediate between the values suggested by Kent (1992) and Reid & Majewski (1993). But note that our results depend neither on $z_{\rm e}$ nor on the particularities of the vertical density distribution. We use disk mass-to-light ratios ($\Upsilon_{\rm d,K}$) such that Kuijken & Gilmore's (1989b) 2-σ range for the local stellar columndensity is spanned. The stellar disk is truncated at (R_0 + 4.5) kpc (Robin, Crézé & Mohan 1992; Freudenreich 1996, 1998).

We now turn to the contribution to the mass models from the interstellar medium. Our location inside the Milky Way means that distances to diffuse components like the ISM are based on a kinematical model. Thus, important properties like the full width at half maximum (FWHM), columndensity, and total mass of the ISM depend on the Galactic constants and the Milky Way's rotation curve. Thus, we re-determine the atomic and molecular gas distributions for each choice of R_0 and Θ_0 . While the columndensities at fractional radius R/R_0 are independent of the choice of R_0 & Θ_0 (Bronfman *et al.* 1988), the total gas mass and the thickness of the gas layer are not. As a result we can do no better than determining the gaseous column-density (Σ_g) at fractional radius R/R_0. Likewise, since the thickness measurement returns an angular size, we can only determine FWHM/R_0 at fractional radiusR/R_0. Physical length-scales for the thickness and Galactocentric radius can be assigned after choosing a value for R_0.

For the inner Galaxy, the H I columndensity was determined from the midplane volume density (Burton 1988) and the observed thickness of the layer (Malhotra 1995). The H I columndensities for $R \gtrsim R_0$ were taken from Wouterloot *et al.* (1990). The H_2 columndensities for the inner and outer Galaxy were copied from Bronfman *et al.* (1988) and Wouterloot *et al.* (1990), respectively**. For the radial profiles of the ISM we neglect the columndensity due to the other phases of the ISM. However, in order to properly take into account all baryonic contributions to the local columndensity, we include 1.4 $M_\odot$ pc^{-2} of ionized hydrogen (Kulkarni & Heiles 1987) *at the Solar position only.* We further include 23.8% helium by mass (Olive & Steigman 1995) to compute the surface densities.

As is commonly done (e.g., van Albada & Sancisi 1986; Kent 1987; Begeman 1989; Lake & Feinswog 1989; Sackett & Sparke 1990; Broeils 1992; Olling 1995; Olling 1996b), we model the dark matter density distribution as a non-singular isothermal spheroid with flattening q, and a density distribution given by:

$$\rho_h(R,z;q) \quad = \quad \rho_0(q) \, \left(\frac{R_c^2(q)}{R_c^2(q) + R^2 + (z/q)^2} \right) \,, \qquad (1)$$

where the halo's core radius ($R_{\rm c}$) and central density (ρ_0) depend on the flattening in such a way that the family of density distributions $\rho_h(q)$ have a rotation curve that is essentially independent of q (Olling 1995). Figure 1 shows the radial distribution of dark matter for three values of R_0, for the range in model parameters as listed in Table 2. Each choice for $h_{\rm d}$ and Σ_* results in a different distribution. The largest DM densities are obtained for large $h_{\rm d}$'s and small Σ_*'s. Even though the central DM density is uncertain by over three orders of magnitude, the local dark matter density is determined rather well: we find

$$\frac{\rho_{\rm DM}(R_0,\Theta_0)}{10^{-3} M_\odot\, {\rm pc}^{-3}} \quad = \quad \frac{11.5 + 3.8 \times (R_0 \ - 7.8) \pm 2}{q\,(26.7/\Omega)^2} \qquad (2)$$

with $\Omega = \Theta_0/R_0$, and where R_0 is in kpc, and Θ_0 in km s^{-1}. The ($\sim 25/q$)% uncertainty arises as a result of the uncertainty in $\Sigma_{tot}^{1.1}$ and Σ_*. For example, taking R_0 = 7.1 kpc, q = 0.71, and using the parameters tabulated in Table 2, we find $\rho_{DM}(R_0)$ = 10.5 m$M_\odot$ pc^{-3}(1 m$M_\odot$ pc^{-3}=

** A graphical representation of the derived gaseous surface density distributions can be found in a related paper on the Galactic & Oort constants (Olling & Merrifield 1997a,1998b). The H_2 columndensities have been re-scaled from the original sources assuming $N({\rm H_2})/W(CO)$ = 2.3 10^{20} cm^{-2} (K km s^{-1})$^{-1}$. We present the radial increase of the thickness of the gas layer in Paper I. The thickness and columndensity of the H I and H_2 are tabulated in Appendix C

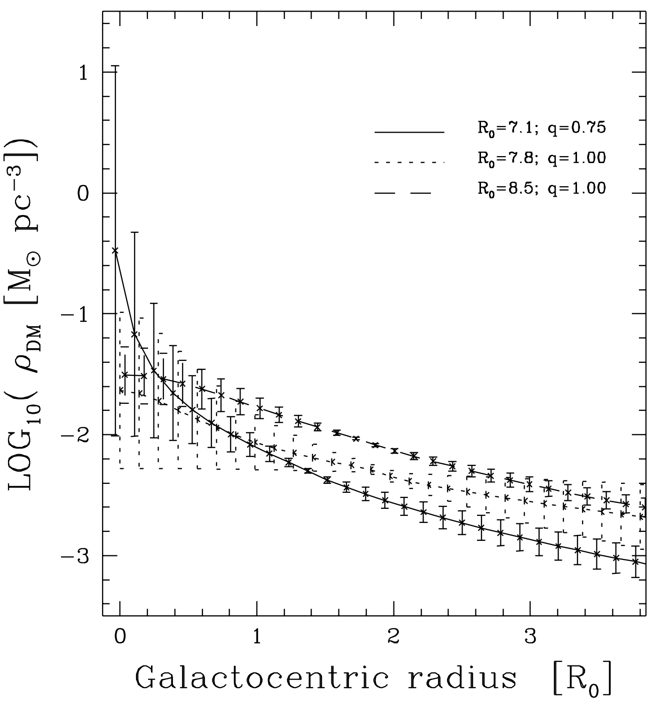

Figure 1. The dark matter midplane density distribution calculated using equation (1) for three values of R_0 and q. The densities scale approximately as $1/q$ (Olling 1995) The error bars represent the full range for the case corresponding to $\Sigma_* = 35 \pm 5\ M_\odot\,\mathrm{pc}^{-2}$, and h_d=2 to 3 kpc. Notice that although the DM density at the Solar circle is relatively well determined, the central density is uncertain by more than three orders of magnitude. Note that we have offset the radial coordinates of the R_0=7.1, and 8.5 kpc models from their true positions (i.e., the R_0=7.8 kpc points) to avoid overlapping symbols.

$10^{-3}\ M_\odot\,\mathrm{pc}^{-3}$). Thus, the $R_0 = 7.1$ model value for the DM matter density compares well with the values given by equation (2) as well as with the observational determination (§3.1).

2.2 Other Dark Matter models

Of course, other mass models can be constructed which represent the radial dark matter density distribution (e.g., van Albada & Sancisi 1986; Navarro, Frenk & White 1996; Dehnen & Binney 1998). However, all viable mass models must share the property that they reproduce the Galactic rotation curve. For a round halo the vertical force approximately equals z/R times the radial force. Since the radial force is approximately the same for all models which reproduce the observed rotation curve, the ensemble of possible models also have approximately equal vertical forces, independent of the exact radial DM density distribution (Olling 1995). In a flattened halo with the same rotation curve, the DM densities are roughly proportional to $1/q$, independent of the radial mass distribution [cf. eqn. (2)]. Thus, our analysis will not be seriously compromised by restricting ourselves to one particular DM density distribution.

3 CONSTRAINING THE DARK MATTER DENSITY

In this section we present two simple analytical models to illustrate the existing correlations between R_0, Θ_0, $\Sigma^{1.1}_{tot}$, Σ_*, q, and σ_g outlined in the Introduction. These models can be used to show how the local stellar kinematics and the H I flaring constrain the dark matter density in the Solar neighbourhood and at $\sim 2\ R_0$. But first we investigate how well the local stellar columndensity is determined and how accurately this determination constrains the dark matter density in the Solar neighbourhood.

3.1 The local stellar columndensity: a constraint?

The Milky Way is a unique galaxy in that we can, at least in principle, determine the local columndensity of stars directly. Once Σ_* is accurately determined, it is possible to establish to what degree the Milky Way disk is maximal, which would provide an important benchmark for external galaxies. Unfortunately this benchmark is not yet available, as the values for Σ_* reported in the literature range from 26 to 145 $M_\odot\,\mathrm{pc}^{-2}$.

Two basic techniques have been employed to determine Σ_*. The direct method involves converting star counts as a function of Galactic coordinates and magnitude to in-situ mass densities. This method is somewhat hampered by uncertainties in the conversion from luminosity to mass, completeness problems in the Solar neighborhood, and binary corrections at large distances. Gould, Bahcall & Flynn (1997; hereafter referred to as GBF97) used deep HST star counts of M-dwarfs at great heights above the plane in combination with a local normalization to infer a stellar columndensity of only $25.8 \pm 3.8\ M_\odot\,\mathrm{pc}^{-2}$. The second, kinematical, method employs the interrelationship between the potential, the vertical density distribution, and the variation of the velocity dispersion with z. Many authors have employed this method, yielding a large range in inferred values for Σ_*. For example, Bahcall (1984b) found Σ_* values of ∼40, ∼52, ∼68, and ∼145 $M_\odot\,\mathrm{pc}^{-2}$ for dark matter distributions that resemble the gaseous disk, an isothermal halo, the thin stellar disk, or the thick stellar disk, respectively. Other authors find values as low as 35 $M_\odot\,\mathrm{pc}^{-2}$ (Kuijken & Gilmore 1989b; Flynn & Fuchs 1994). Methods that combine the two primary methods exist as well (Bienaymé, Robin & Crézé 1987; Crézé, Robin & Bienaymé 1989). In Appendix A we simulate the kinematic determination of the stellar columndensity with the aid of Galaxy models –taken from Table 2– for which we know the exact force law. Our results are in complete agreement with the findings of previous authors: the "vertical disk-halo conspiracy" can only be resolved if high-z stellar kinematical data are included and/or if additional assumptions are made (e.g., a "reasonable" value for the DM density). Typical values for the mass of the *stellar* disk are 52 (Bahcall 1984b), 35 ± 5 (Kuijken & Gilmore 1989b) and 37 ± 13 $M_\odot\,\mathrm{pc}^{-2}$(Flynn & Fuchs 1994).

Considering the uncertainties in the kinematical estimates of the total mass of the disk, it might be preferable to

Table 2. Disk & halo parameters. A log for a representative sample of models for which *exact* flaring curves are calculated. The meaning of the columns is as follows: 1) γ, the degree to which the stellar disk is maximal; 2) scale-length of stellar disk (kpc); 3&4) bulge & disk K-band mass-to-light ratios; 5&6) stellar columndensity & total columndensity within 1.1 kpc of the plane ($M_\odot\,\mathrm{pc}^{-2}$); 7&8) core radius (kpc) and central density ($10^{-3}\ M_\odot\,\mathrm{pc}^{-3}$) of the dark halo, assuming q=1 (multiply by $\approx 1/q$ to scale to different values of q, for a more exact scaling, see Olling 1995); 9&10) dark halo flattening as inferred from the H I flaring ($q_{\mathrm{H\ I}}$) and the local columndensities ($q_{1.1}$).

γ	h_d	$\Upsilon_{\mathrm{b,K}}$	$\Upsilon_{\mathrm{d,K}}$	Σ_*	$\Sigma^{1.1}_{tot}$	R_c	ρ_0	$q_{\mathrm{H\ I}}$	$q_{1.1}$
R_0=6.8,	Θ_0=182								
0.80	2.0	0.55	0.422	30.21	62.48	2.39	73.8	0.630 ± 0.107	0.561 ± 0.175
0.86	2.0	0.55	0.488	34.92	66.02	3.54	35.6	0.687 ± 0.113	0.664 ± 0.226
0.92	2.0	0.55	0.558	39.96	68.72	6.09	14.6	0.699 ± 0.120	0.753 ± 0.295
0.64	2.5	0.55	0.327	29.58	63.56	1.32	246.3	0.687 ± 0.152	0.620 ± 0.183
0.70	2.5	0.55	0.392	35.39	68.84	1.86	125.1	0.717 ± 0.134	0.826 ± 0.268
0.75	2.5	0.55	0.449	40.63	73.40	2.45	73.0	0.674 ± 0.127	1.061 ± 0.371
0.56	3.0	0.55	0.306	30.21	64.34	0.70	853.9	0.740 ± 0.181	0.651 ± 0.194
0.60	3.0	0.55	0.351	34.68	68.6	1.00	421.0	0.770 ± 0.159	0.820 ± 0.261
0.65	3.0	0.55	0.412	40.70	74.18	1.44	201.9	0.762 ± 0.137	1.114 ± 0.382
R_0=7.1,	Θ_0=189								
0.82	2.0	0.45	0.482	29.71	61.94	2.73	62.7	0.625 ± 0.132	0.544 ± 0.165
0.89	2.0	0.45	0.568	35.00	65.66	4.53	25.5	0.624 ± 0.116	0.636 ± 0.214
0.95	2.0	0.45	0.647	39.87	66.74	9.77	8.6	0.679 ± 0.104	0.603 ± 0.239
0.65	2.5	0.55	0.370	29.66	62.60	1.13	340.1	0.727 ± 0.159	0.581 ± 0.173
0.71	2.5	0.55	0.441	35.39	67.76	1.66	158.2	0.738 ± 0.161	0.765 ± 0.250
0.76	2.5	0.55	0.506	40.55	72.26	2.25	86.4	0.823 ± 0.223	0.999 ± 0.356
0.56	3.0	0.55	0.333	29.73	61.82	0.20	9884.5	0.735 ± 0.181	0.550 ± 0.168
0.61	3.0	0.55	0.395	35.28	67.10	0.55	1343.6	0.703 ± 0.158	0.734 ± 0.243
0.63	3.0	0.55	0.421	37.63	69.32	0.71	802.8	0.786 ± 0.210	0.843 ± 0.290
R_0=7.8,	Θ_0=207								
0.92	2.0	0.45	0.687	29.80	64.60	9.51	15.4	1.003 ± 0.119	0.616 ± 0.162
0.72	2.5	0.75	0.492	29.80	64.76	4.59	47.9	1.744 ± 0.553	0.963 ± 0.240
0.78	2.5	0.75	0.577	34.97	71.00	5.81	32.6	1.616 ± 0.443	1.065 ± 0.260
0.84	2.5	0.75	0.669	40.56	77.66	8.01	20.6	1.461 ± 0.337	1.191 ± 0.331
0.59	3.0	0.75	0.430	30.46	66.54	2.84	103.4	1.623 ± 0.451	0.973 ± 0.244
0.61	3.0	0.75	0.460	32.56	68.06	3.02	91.7	2.019 ± 0.758	1.026 ± 0.260
0.68	3.0	0.75	0.572	40.46	77.54	3.81	59.3	1.810 ± 0.753	1.327 ± 0.364
R_0=8.5,	Θ_0=227								
0.76	2.5	0.60	0.670	30.66	78.68	6.81	39.1	2.922 ± 0.863	1.169 ± 0.252
0.81	2.5	0.60	0.761	34.83	80.43	8.34	28.9	2.512 ± 0.608	1.228 ± 0.279
0.86	2.5	0.60	0.857	39.26	81.28	11.10	19.9	1.931 ± 0.366	1.256 ± 0.306
0.59	3.0	0.85	0.486	27.23	76.53	5.09	60.2	1.424 ± 0.156	1.165 ± 0.193
0.67	3.0	0.85	0.627	35.11	82.49	6.20	43.2	1.498 ± 0.183	1.364 ± 0.213
0.75	3.0	0.85	0.785	44.00	88.53	8.07	28.9	1.475 ± 0.197	1.641 ± 0.159

use the direct star count method to determine Σ_*. The latest results by GBF97 imply Σ_*=25.8 ± 3.8 $M_\odot\,\mathrm{pc}^{-2}$. However, the local space density of stars found by these authors [(33.2 ± 8.6) m$M_\odot\,\mathrm{pc}^{-3}$] is somewhat lower than the values reported in the literature [(43 ± 15)[††] m$M_\odot\,\mathrm{pc}^{-3}$]. This suggests that GBF97 underestimated Σ_* by a factor of 1.4 ± 0.2, and so we find Σ_* = 36 ± 5 $M_\odot\,\mathrm{pc}^{-2}$: the star count method yields a value for Σ_* which is remarkably close to the kinematical estimates. However, it is quite interesting to note that the total matter density in the Solar neighbourhood as inferred from recent Hipparcos data (Crézé *et al.* 1998) of 76 ± 15 m$M_\odot\,\mathrm{pc}^{-3}$ favours a local stellar volume density which is even smaller than reported by GBF97. After subtracting the density of the ISM (see Table 1) and the local DM density [eqn. (2)] we find $\rho_*(R_0) \sim 21 \pm 15$ m$M_\odot\,\mathrm{pc}^{-3}$. Note that even lower values for ρ_* result if large values for the Galactic constants and/or Ω are chosen, while

[††] The average of: ρ_* = 46 (Wielen 1974), 50.8 (Bahcall 1984a; Bahcall, Flynn & Gould 1992), 45 m$M_\odot\,\mathrm{pc}^{-3}$ [Crézé *et al.* (1998).

smallish Galactic constants and Ω decrease the local DM density. To summarize, a "reasonable" value for Σ_* might be 35 $M_\odot\,\mathrm{pc}^{-2}$, and we suggest a "consensus" error of 10 $M_\odot\,\mathrm{pc}^{-2}$. Subtracting the columndensities of the stellar and ISM distributions, dark matter in the Solar neighbourhood amounts to $\Sigma_h = (24.5 \pm 11)\ M_\odot\,\mathrm{pc}^{-2}$ within 1.1 kpc of the plane, or a local dark matter density of 11 ± 5 m$M_\odot\,\mathrm{pc}^{-3}$.

3.2 The connection between dark and luminous matter in the Solar neighbourhood

In the previous section we have seen that the contribution of the stellar and dark matter components to the local disk mass cannot be clearly segregated. Thus the observed value for $\Sigma^{1.1}_{tot}$ implies that Σ_* and Σ_h are highly correlated: a low stellar column implies a large amount of dark matter, and vice versa. Since the dark matter density depends on the amplitude of the rotation curve and the halo's flattening, these parameters are in turn related to Σ_*. Below we investigate the relations between $\Sigma^{1.1}_{tot}$, Θ_0, Σ_* and q in some detail.

Integrating equation (1) with respect to z and applying equation (A4) from Olling (1995), we find the columndensity of dark matter within z of the Galactic plane as a function of q:

$$\Sigma^z_h(q) \;=\; \frac{2q\rho_0(q)R^2_c(q)}{\sqrt{R^2_c(q)+R^2}}\arctan\left(\frac{z/q}{\sqrt{R^2_c(q)+R^2}}\right) \qquad (3)$$

$$= \frac{V^2_{h,\infty}\sqrt{1-q^2}}{2\pi G\sqrt{R^2_c(q)+R^2}\arccos q}\arctan\left(\frac{z/q}{\sqrt{R^2_c(q)+R^2}}\right), \qquad (4)$$

with $V_{h,\infty}$ the asymptotic rotation velocity of the round dark halo. For each of our self-consistent mass models we can calculate $\Sigma^{1.1}_{tot}(q)$ and find that it obeys a simple power law relation:

$$\Sigma^{1.1}_{tot}(q) \;=\; \Sigma^{1.1}_h(q) + \Sigma_* + \Sigma_g \qquad (5)$$

$$\approx \Sigma^{1.1}_{tot}(q=1)\times q^{-p}\,. \qquad (6)$$

The dependence of $\Sigma^{1.1}_{tot}$ on the other parameters of the model parameters are combined into the index p (with $p \sim 0.05-0.45$)‡‡. The halo flattening inferred from the local stellar kinematics ($q_{1.1}$) is then found by equating $\Sigma^{1.1}_{tot}(q)$ with the observed value and solving equation (6) for q

$$q_{1.1} \;=\; \left(\frac{\Sigma^{1.1}_{tot}(q=1)}{71\pm 6}\right)^{\frac{1}{p}}\,. \qquad (7)$$

Equations (4), (6) and (7) can be combined to find the dependence of $q_{1.1}$ on the Galactic constants. Neglecting R_c, equating $V_{h,\infty}$ with Θ_0, and retaining only the DM contribution to the total surface density, we find:

$$q_{1.1} \;\propto\; (\Theta_0/R_0)^{2/p}\,. \qquad (8)$$

Qualitatively, this is the functional dependence we expect: increasing Θ_0 at constant R_0 would increase the required amount of DM, which has to be counteracted by increasing $q_{1.1}$ to retain the same $\Sigma^{1.1}_{tot}$. Likewise, increasing R_0 would place the Sun in a lower density region of the halo, which needs to be compensated by decreasing $q_{1.1}$. Furthermore, given the small values of p, $q_{1.1}$ depends very strongly upon the Galactic constants.

If we include the other components to the total columndensity, the halo flattening inferred from the local stellar kinematics is a function of $\Sigma_*, \Sigma_g(R_0), R_c$ and the Galactic constants. In Appendix B we present some examples of correlations between the Galactic constants, Σ_*, Θ_0 and $q_{1.1}$ derived from equation 5 which take all three mass components into account. These examples show that the $\Sigma^{1.1}_{tot}$ constraint implies highly flattened DM halos for small values of Θ_0.

3.3 Constraints from the thickness of the gas layer

In an idealized picture, the equilibrium thickness of the gas in the Milky Way depends only on the gas temperature and the form of the potential in which it has settled. Thus, the observed FWHM of the gas layer can be used to constrain the potential of the Galaxy. In Paper I we present evidence that the interstellar medium beyond the optical disk comprises only a single, iso-thermal component. We therefore adopt the same assumption in the analysis below. In this section we will expand our analysis to include the effects of non-thermal pressure gradients.

If the gas layer is in a steady state and we assume that only thermal and random motions of the gas contribute to the pressure in the ISM, the thickness of the gas layer follows from the equation of hydrostatic equilibrium:

$$\frac{d\ {\sigma_g}^2\rho_g(z)}{dz} \;=\; \rho_{\rm g}(z)\ K_{\rm z}(z)\,, \qquad (9)$$

where σ_g, $\rho_g(z)$, and $K_{\rm z}$ are the gaseous velocity dispersion and volume density, and the vertical force per unit mass, respectively. The vertical force is commonly determined using a "local approximation" which $K_{\rm z}$ follows from the the poisson equation and the local mass densities and the radial gradient of the rotation curve. However, this approach is known to fail in regions where either the mass densities or the rotation curve, or both, have steep gradients. Further, the local approach neglects any variation of the circular speed with height above the plane. These problems can be overcome by calculating K_z from the global mass distribution (the "global approach", Olling 1995). As mentioned in section 2, we combine the exactness of the global approach with the speed of the local approximation for optimal results.

If we employ the local approximation the dependencies

‡‡ The values for $\Sigma^{1.1}_{tot}(q)$, $\Sigma^{1.1}_{tot}(q=1)$ and p are different for each combination of the Galactic constants, the stellar disk mass and scale-length. p can be determined from a fit to equation (6), where we determine $\Sigma^{1.1}_{tot}(q)$ for several models with varying q's. Note that we also use equation (6) to extrapolate into the prolate regime, with the exponent p as determined for the oblate models.

between the various parameters of the model become apparent. For example, when the potential is dominated by mass component i, equation (9) can be solved for the thickness of the gas layer:

$$\mathrm{FWHM_i} \propto \frac{\sigma_g}{\sqrt{4\pi G \rho_i}}\,, \tag{10}$$

where the proportionality constant depends on the vertical density distribution of the dominant contributor to the local vertical potential (Olling 1995). For example, in case the gas is fully self-gravitating, the width is given by:

$$\mathrm{FWHM_g} \approx 0.158 \frac{{\sigma_g}^2}{\Sigma_g}\,, \tag{11}$$

and if the dark matter halo dominates the potential, we find:

$$\mathrm{FWHM_h} \approx \sqrt{\frac{13.5\ q}{1.4+q}} \frac{\sigma_g}{V_{\mathrm{h},\infty}} \sqrt{R_{c,1}^2 + R^2}\,, \tag{12}$$

where $R_{c,1}$ is the core radius of the equivalent round halo (Olling 1995). All distances and widths are in kpc, and all velocities in km s^{-1}. The thickness of the gas layer in the combined potential of several mass components can be solved analytically in the form of an integral equation, but requires an iterative solution procedure (Olling 1995, Appendix C). A further approximation is possible. Following Olling (1995, Appendix D) we use:

$$\frac{1}{\mathrm{FWHM}^2{}_\mathrm{g}} \approx \sum_i \frac{w_i}{\mathrm{FWHM}^2{}_\mathrm{i}}\,, \tag{13}$$

where the weighting factors w_i reflect the relative importance of component i in the region where the gas resides§§. Solving equation 13, for $q_{\mathrm{H\ I}}$, taking $V_{h,\infty} \approx \Theta_0$ and neglecting $R_{c,1}$, we find:

$$q_{\mathrm{H\ I}}\,(2R_0) \approx \frac{1.4}{2.4\left(\frac{1}{(\zeta 2R_0)^2} - \left(\frac{\Sigma_g w_g}{0.159{\sigma_g}^2}\right)^2 \left(\frac{2R_0}{w_h}\frac{\sigma_g}{\Theta_0}\right)^2\right) - 1}\,, \tag{14}$$

with $\zeta(R) = \mathrm{FWHM_{obs}}/R$ (~ 0.07 for the outer Milky Way), and where Σ_g, w_g, and w_h have to be evaluated at $R = 2R_0$ (see footnote §§). From this equation we infer that the contribution of the self-gravity of the gas depends strongly on the gaseous velocity dispersion: low σ_g values result in a more negative self-gravity contribution to the denominator, and hence leads to a larger inferred $q_{\mathrm{H\ I}}$. As we have already mentioned, the self-gravity of the gas is an important component as it reduces the width of the gas layer by approximately 45%. A further simplification can be made by neglecting the gaseous self-gravity as well, we find:

$$q_{\mathrm{H\ I}} \approx \frac{1.4[\zeta(R)\Theta_0]^2}{13.5{\sigma_g}^2 - [\zeta(R)\Theta_0]^2}\,, \tag{15}$$

$$q_{\mathrm{H\ I}} \propto \frac{{\Theta_0}^2}{{\sigma_g}^2}\,, \tag{16}$$

where the second line arises because the first term in the denominator dominates. The dependence of $q_{\mathrm{H\ I}}$ on Θ_0 and σ_g are indeed as outlined in the Introduction. Also note that, due to the quadratic nature of the proportionalities, the observed flaring and the small allowed range of $q_{\mathrm{H\ I}}$ constrain Θ_0 and σ_g rather tightly.

Comparing equations (8) and (16) we see that the constraints on the halo shape arising from the local stellar kinematics and the H I flaring the have rather different R_0 and Θ_0 dependencies. Thus, it is indeed possible to learn more about the Galactic dark matter distribution by combining these two constraints. Further, unlike the stellar kinematical method, the constraints from the H I flaring is independent of Σ_* since it arises at $R \sim 2R_0$, beyond the truncation of the stellar disk.

However, the usefulness of equations (14)-(16) are limited to the real of illustrating the dependence of $q_{\mathrm{H\ I}}$ on the model parameters since several important aspects are treated too simplistic. First, neglecting R_c and equating $V_{h,\infty}$ with Θ_0 is only seldomly warranted. Second, depending on the slope of the rotation curve, an error of order $\pm$ 20% is made in the inferred $q_{\mathrm{H\ I}}$. We therefore do not recommend using equations (14)-(16) "as is" to determine $q_{\mathrm{H\ I}}$ directly. In all our calculations we employ equation (13) where we take all mass components fully into account, without any further simplifications¶¶.

4 THE EFFECTS OF A LARGER GASEOUS VELOCITY DISPERSION

Equations (9)-(14) show that $q_{\mathrm{H\ I}}$ is a function of σ_g, Θ_0 and R_0. On the other hand, the halo flattening inferred from the local stellar kinematics is a function of the Galactic constants and Σ_*. In a self-consistent model, $q_{1.1} \equiv q_{\mathrm{H\ I}}$, so that strong inter-relations are imposed among the currently ill-determined values of R_0, Θ_0, Σ_* and σ_g.

Below we investigate how the inferred halo flattening and stellar columndensity depend upon our choice of σ_g. The value of σ_g can have significant effects on the inferred values of q and Σ_*. For example, in Paper I we assumed that the true velocity dispersion equals 9.2 km s^{-1}, and found an

§§ See Olling (1995) for details. For the Milky Way we will use: $w_g = ((1.24\Sigma_g + 1.55 W_h \times (\rho_h + \rho_r))/(\Sigma_g + W_h \times (\rho_h + \rho_r))$, $w_h = (1.0 + 0.35 \times \exp(-1.7 W_h \rho_h/\Sigma_g))$, and $w_r = (1 + w_h)/2$. ρ_h is the local dark matter density, the "rotational" density, $\rho_r (\equiv \frac{-1}{2\pi \mathrm{G}} \frac{V_{\mathrm{rot}}}{R} \frac{dV_{\mathrm{rot}}}{dR})$, arises due to the slope of the rotation curve. W_h equals $\mathrm{FWHM_h}/2.35$ as calculated from equation 12. For example, at R$\sim 2R_0$, $\Sigma_g \sim 7.7$ and $(\Sigma_h, \Sigma_r) = (3.6, -0.30), (5.3, -0.17), (6.0, -0.37)$ $M_\odot\,\mathrm{pc}^{-2}$ for R_0=7.1, 7.8, and 8.5 kpc, respectively. These values lead to weights which are almost independent of R_0: $w_g \sim 1.4, w_h \sim 1.2, w_r \sim 1.1$. These weightings embody the calibration of the local approximation for the outer Milky Way.

¶¶ For many combinations of parameters, a round halo is too dense to explain the observed flaring (cf. Fig. 2). Albeit not entirely correct, we will determine the halo's contribution to the potential using equation (12) in those cases.

upper limit to the local rotation speed of about 190 km s^{-1}. Further, models with the IAU recommended Galactic constants have prolate dark halos ($q \sim 1.9$) and require a rather high local stellar columndensity of $\sim$55 $M_\odot$ pc^{-2}. Increasing σ_g would bring q and Σ_* down to more acceptable levels, and it might thus be worthwhile to treat σ_g as a free rather than as a fixed parameter.

However, observations of external galaxies imply that the velocity dispersion *declines* slightly in the radial range over which the Milky Way's flaring has been measured, by a factor 1.12 $\pm$ 0.12 (van der Kruit & Shostak 1984; Dickey, Hanson & Helou 1990; Kamphuis 1993; Côté 1995; Olling 1996b; Sicking 1997). Furthermore, there is some evidence that σ_g in the outer Galaxy equals the value inside the Solar circle (Blitz & Spergel 1991). Also, one would expect that a change in gaseous velocity dispersion would be reflected in a change of the residual motions of young stars with respect to the mean streaming field. Such changes have not been observed, neither in B stars nor in Cepheids (Brand & Blitz 1993; Pont, Queloz, Bratchi & Mayor 1997). Thus, an increase in gaseous velocity dispersion beyond the Solar circle is not likely.

4.1 Non-thermal pressure terms

In Paper I we argued that the ISM beyond the optical disk comprises a single, iso-thermal component. We now investigate the possibility that non-thermal pressures have to be included in the hydrostatic balance.

It is estimated that in the Solar neighbourhood thermal motions, cosmic rays, and magnetic fields contribute about equally to the interstellar pressure (Spitzer 1978; Kulkarni & Heiles 1987). The equation of hydrostatic equilibrium can be written as:

$$\rho_{\rm g}(z)\ K_{\rm z}(z) \quad = \quad \frac{dP_G}{dz} + \frac{dP_B}{dz} + \frac{dP_C}{dz} = \frac{dP_{tot}}{dz} \qquad (17)$$

with $P_G = {\sigma_g}^2 \rho_g(z)$ the thermal gas pressure, $P_B = B^2/8\pi$ the magnetic field pressure, and $P_C = 1/3 U_C$ is the pressure due to cosmic rays with energy density U_C. Taking the scale-heights of the kinetic, magnetic and cosmic ray energy density to be z_G, z_B, and z_C, we write the pressure gradients as $\frac{dP_G}{dz} = \frac{P_G}{z_G}$, $\frac{dP_B}{dz} = \frac{P_B}{z_B}$, and $\frac{dP_C}{dz} = \frac{P_C}{z_C}$. In the Solar neighborhood the scale-heights z_B and z_C are κ_B and κ_C times larger than the gaseous scale-height [$\kappa_B \sim 10, \kappa_C \sim 4$; (e.g.; Kulkarni & Heiles 1987; Rupen 1991)]. Following Spitzer (1978) we assume that the non-thermal pressure terms are proportional to the kinetic pressure: $P_B = \alpha_B P_G$ and $P_C = \alpha_C P_G$, with $\alpha_B \sim 0.25$ and $\alpha_C \sim 0.4$ in the Solar neighborhood (Spitzer 1978). Using these parameterizations we find:

$$\rho_{\rm g}(z)\ K_{\rm z}(z) \quad \approx \quad {\sigma_g}^2 \left(1 + \frac{\alpha_B}{\kappa_B} + \frac{\alpha_C}{\kappa_C}\right) \frac{d\rho_G}{dz} \qquad (18)$$

$$\approx \quad (\sigma_g')^2 \frac{d\rho_G}{dz} \qquad (19)$$

where we have lumped all terms contributing to the hydrostatic balance into a single unknown, the effective velocity dispersion σ_g'. With the above simplifications and equations (10) and (15), it becomes possible to estimate the effects of non-thermal pressure support on the thickness of the gas layer and the inferred shape of the dark matter halo:

$$\left.\frac{\rm FWHM_{GBC}}{\rm FWHM_G}\right|_{R_0} \approx \frac{\sigma_g'}{\sigma_g} = \sqrt{1 + \frac{\alpha_B}{\kappa_B} + \frac{\alpha_C}{\kappa_C}} \sim 1.06 \qquad (20)$$

$$\left.\frac{q_{GBC}}{q_G}\right|_{R_0} \approx \left(\frac{\sigma_g}{\sigma_g'}\right)^2 \sim 0.89\,, \qquad (21)$$

where the subscripts GBC indicates that the gaseous, magnetic and cosmic ray terms are taken into account in the hydrostatic balance of the gas layer. Thus, neglecting the non-thermal contribution to the pressure balance in the local ISM leads to a gas layer width which is under-estimated by a few percent only. Similarly, a slightly more flattened halo is required if non-thermal pressure support were important in the Solar neighborhood. Since we only employ the H I thickness measurements at large radii as a constraint in our mass models, let us try to guess the value of σ_g' at $\sim 2R_0$.

The gas density in the outer Galaxy is about four times smaller than at R_0 as a result of the decrease in columndensity (factor 2) and the increase in thickness (factor 2). To make a conservative estimate as to the importance of the non-thermal terms at large distances, we assume that the magnetic field strength, the cosmic ray energy density and their vertical gradients equal the values in the Solar neighbourhood. Furthermore, we assume that σ_g remains unchanged. With these assumptions, the α values at $2R_0$ are four times larger than at $R = R_0$, while the κ values are decreased by a factor two. Thus, the effective velocity dispersion and the inferred halo shape are strongly affected:

$$\left.\frac{\sigma_g'}{\sigma_g}\right|_{2R_0} \quad = \quad \sqrt{1 + \frac{4\alpha_B(R_0)}{\kappa_B(R_0)/2} + \frac{4\alpha_C(R_0)}{\kappa_C(R_0)/2}} \sim \sqrt{2} \qquad (22)$$

$$\left.\frac{q_{GBC}}{q_G}\right|_{2R_0} \quad \approx \quad \left(\frac{\sigma_g}{\sigma_g'}\right)^2 \sim 0.5\,. \qquad (23)$$

On the basis of this over-estimation, it might be that the gas layer is significantly out of thermal equilibrium at large radii. Do we expect this to be the case? Two effect reduce the importance of the non-thermal contribution. First, the B-field is probably co-spatial, "frozen in", with the ionized part of the ISM which' scale-height has most likely doubled at $R = 2R_0$ (like the H I). Thus, the Solar neighbourhood value for $\kappa_B(2R_0)$ should be used in equation (22). Second, radio-continuum measurements of external galaxies suggest that high cosmic ray fluxes are closely associated with the sites of star formation (Bicay & Helou 1990). Since active star-formation ceases to exist beyond $\sim 1.5R_0$, the α_C-term in eqn. (22) vanishes. Thus, in a more realistic treatment of the non-thermal pressure terms, their effect on the vertical equilibrium of gas at large radii is much reduced:

$$\left.\frac{\sigma_g'}{\sigma_g}\right|_{2R_0} \quad = \quad \sqrt{1 + \frac{4\alpha_B(R_0)}{\kappa_B(R_0)}} = \sqrt{1.1} \sim 1.05 \qquad (24)$$

$$\left.\frac{q_{GBC}}{q_G}\right|_{2R_0} \approx \left(\frac{\sigma_g}{\sigma_g'}\right)^2 \sim 0.9\,. \qquad (25)$$

Further, if the magnetic field strength decreases with Galactocentric radius, the above estimates should be even closer to unity. Thus realistic estimates of the importance of non-thermal pressure terms in the equation of hydrostatic equilibrium indicate that the the thickness of the H I layer is not much affected, neither in the inner, nor in the outer Galaxy.

And finally it is worth mentioning that there exist both theoretical and empirical evidence that non-thermal pressure support is small even when simplified calculations indicate that they may dominate P_G. From a theoretical perspective one finds that the vertical balance is only affected if the magnetic field is horizontally stratified, a configuration that is unstable (Parker 1966), and which is thus not expected to exist on a global scale in the Milky Way. In fact, 3D simulations of the growth of the Parker instability show that the gas is almost entirely supported by thermal pressure within the first four scale-heights (Kim, Hong, Ryu & Jones 1998). On the observational side, Rupen (1991) presents evidence that the non-thermal pressure gradients equal 400% of the thermal pressure gradient in NGC 891, and 50% in NGC 4565. Since the luminous mass distributions in these galaxies are very similar, one would expect very different gas layer widths if non-thermal effects were indeed important. In fact, these two galaxies have almost indistinguishable flaring curves, and we can conclude that thermal pressure gradients dominate (Rupen 1991; Olling 1996a).

To summarize, simplified theoretical considerations indicate that non-thermal pressure support could dominate the hydrostatic balance if extreme assumptions about the magnetic field geometry and the cosmic ray energy density are made. More realistic assumptions regarding P_B and P_C, as well as observational data suggests the contrary.

In the next paragraph we will investigate the effects of significant non-thermal pressure support by treating the gaseous velocity as an unknown, notwithstanding the indications that non-thermal pressure support is actually small in the outer Galaxy. Based on the arguments presented above, we expect σ_g' to lie between $\sim$0.85 and $\sqrt{2}$ times the default value of 9.2 km s^{-1}, while a more realistic upper limit to σ_g'/σ_g would be 1.05 [cf. eqn. (24)].

4.2 Constraints on the pressure term

In this section we address the question as to how the interrelations between the Galactic constants, Σ_* and q are affected when assuming that σ_g is unknown. We follow the procedure to determine the halo flattening as outlined in the Introduction (and Paper I) for several trial values of σ_g ($\sigma_g' = 8.0, 8.6, 9.2, 9.9, 10.5, 12$ and 14 km s^{-1}), and on the same $R_0 - \Theta_0$ grid as in Paper I. As predicted by equation (16), the inferred halo flattening and stellar columndensity are rather sensitive to the adopted value of σ_g'. In figure 2 we present q (dotted lines) and Σ_* (long dashed lines) as calculated for increasing values of σ_g', from left to right, and from top to bottom. The oblate region of parameter space, below the heavy dash-dotted line, is strongly restricted if $\sigma_g'/\sigma_g < 1$ (lower-left panel), while essentially the whole range of the Galactic constants is allowed if the effective dispersion is as large as 12 km s^{-1} (upper-right panel). Furthermore, if the H I flaring requires a more highly flattened halo, $\Sigma_h^{1.1}$ increases at the Solar circle, which in turn requires a smaller Σ_* [cf. eqn (5)]. From these figures we can also infer that the mass of the stellar disk, if measured accurately, constrains the allowed range of σ_g'.
Values for σ_g' that are as much as 30% larger than the default value (upper right panel of Fig. 2) are completely excluded because of the very small stellar disk masses required. On the other hand, lower velocity dispersions need lower density (rounder) halos and hence a more massive stellar disk, for given Galactic constants. This is indeed what is observed in the lower-left panel of Fig. 2 for $\Theta_0 \gtrsim 175$ km s^{-1}. However, below $\Theta_0 \sim 175$ km s^{-1}, the situation is much more chaotic (extreme negative values for Σ_* and q), which is the result of the fact that the H I flaring and the stellar kinematical constraints are mutually exclusive (Appendix B). In fact, an effective velocity dispersion $\lesssim 8$ km s^{-1} is essentially ruled out.

4.3 Other Constraints

In order to take all constraints properly into account, we should present a three dimensional plot with R_0, Θ_0 and σ_g' as the axes. Because this is a little tedious, we opt for to determine the halo flattening and Σ_* along lines of constant Ω. We select Ω values which bracket the uncertainty of the proper motion of SgrA* (Reid *et al.* 1999). In each of the three panels of Figure 3 ($\Omega = 29.9, 27, 4, 24.9$ km s^{-1}kpc^{-1}, from top to bottom) we present contours of constant halo flattening by dotted lines as a function of R_0 and σ_g'. The heavy dashed-dotted line is the round-halo contour. The hashed parts of the diagram depict regions of parameter space where $\Sigma_* = 35 \pm 5\ M_\odot\,\mathrm{pc}^{-2}$ (heavy horizontal hash) and $\Sigma_* = 27.8 \pm 3.8\ M_\odot\,\mathrm{pc}^{-2}$ (light vertical hash). These columndensity ranges correspond to the stellar disk mass as determined by KG89 and GBF97, respectively. In figure 3 we also plot our estimate to the upper limit of the non-thermal pressure support ($\sigma_g' \sim 1.05\sigma_g$) as the thick horizontal line. The cross at $(R_0, \sigma_g') = (7.2, 9.2)$ corresponds to the value of R_0 derived from the Oort constant (Olling & Merrifield 1998) and the standard value of the gaseous velocity dispersion.

A general feature of these diagrams is that flatter halos are found in regions with large values of σ_g'. This arises naturally from the fact that a stronger gravitational pull is needed to constrain a gas layer with additional pressure support, for a given observed thickness [see also eqn. (12)]. These figures also clearly show that regions with large DM densities, due to either large Θ_0 or small q, have low stellar columndensity in the Solar neighbourhood. We can seen that significant non-thermal pressure support, which we define as $\sigma_g' = \sqrt{2}\sigma_g \sim 13$ km s^{-1}, requires very highly flattened dark matter halos *and* very small stellar columndensities in

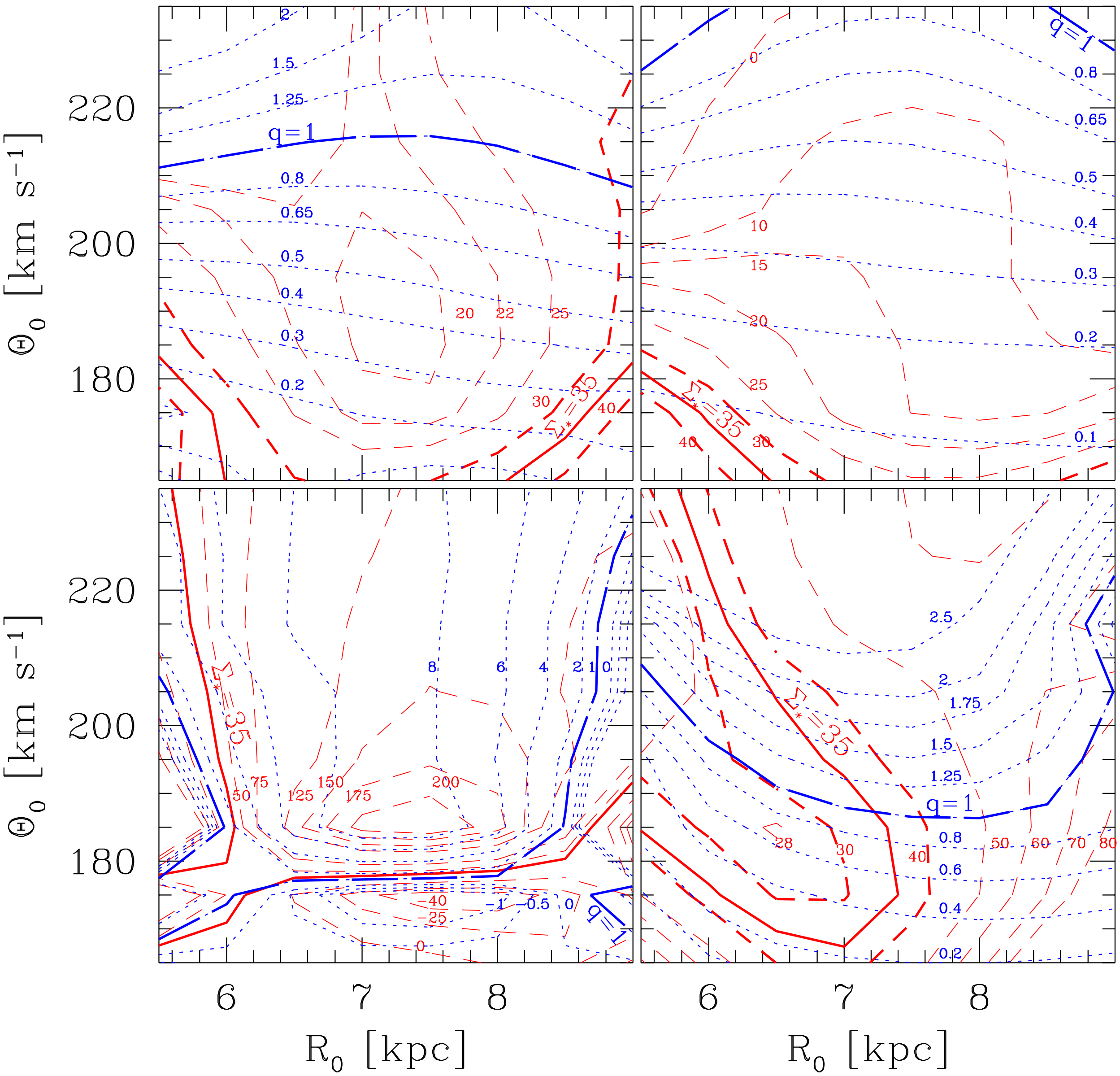

Figure 2. Here we present the *mutually consistent* set of Galactic constants, stellar columndensity in the Solar neighborhood (Σ_*; long dashed lines) and halo flattening (q; dotted lines). The individual panels show the results of the calculation for several values of σ_g'/σ_g: 0.85 (σ_g'=8 km s^{-1}, lower left), 1.0 (σ_g'=9.2 km s^{-1}, lower right), 1.15 (σ_g'=10.5 km s^{-1}, upper left), and 1.30 (σ_g'=12 km s^{-1}, upper right). The oblate-prolate boundary is indicated by the heavy dash-dotted line. The heavy full line and the heavy dashed line corresponds to KG89's determination of Σ_*, and the $\pm 1-\sigma$ values. The upper limit of GBF97's determination of the stellar columndensity corresponds to the $\Sigma_* \sim 30\ M_\odot\ \mathrm{pc}^{-2}$ contour. Both the halo flattening and stellar column are determined to $\sim 6\%$ accuracy. Because the Galactic constants, Σ_*, and q have to be mutually consistent one cannot arbitrarily choose the four parameters. Fixing one of the four parameters severely restricts the other three. Any two parameters follow immediately from any choice of the other two, for a given σ_g.

the Solar neighbourhood. Such strong non-thermal pressure support is thus ruled out.

Several other generic conclusions can be drawn from figure 3. First, highly flattened halos are only possible for realistic values of Σ_* if $R_0 \lesssim 7$ kpc, and only for small values of Ω. Second, large values for R_0, an acceptable stellar columndensity, and an oblate halo occur only if the angular velocity of the Milky Way is small, whatever the value of the effective velocity dispersion. Third, the extra degree of freedom associated with σ_g' does not greatly influence the inferred halo flattening if a good constraint on Σ_* can be used. And finally, the combined constraints set by the observed stellar

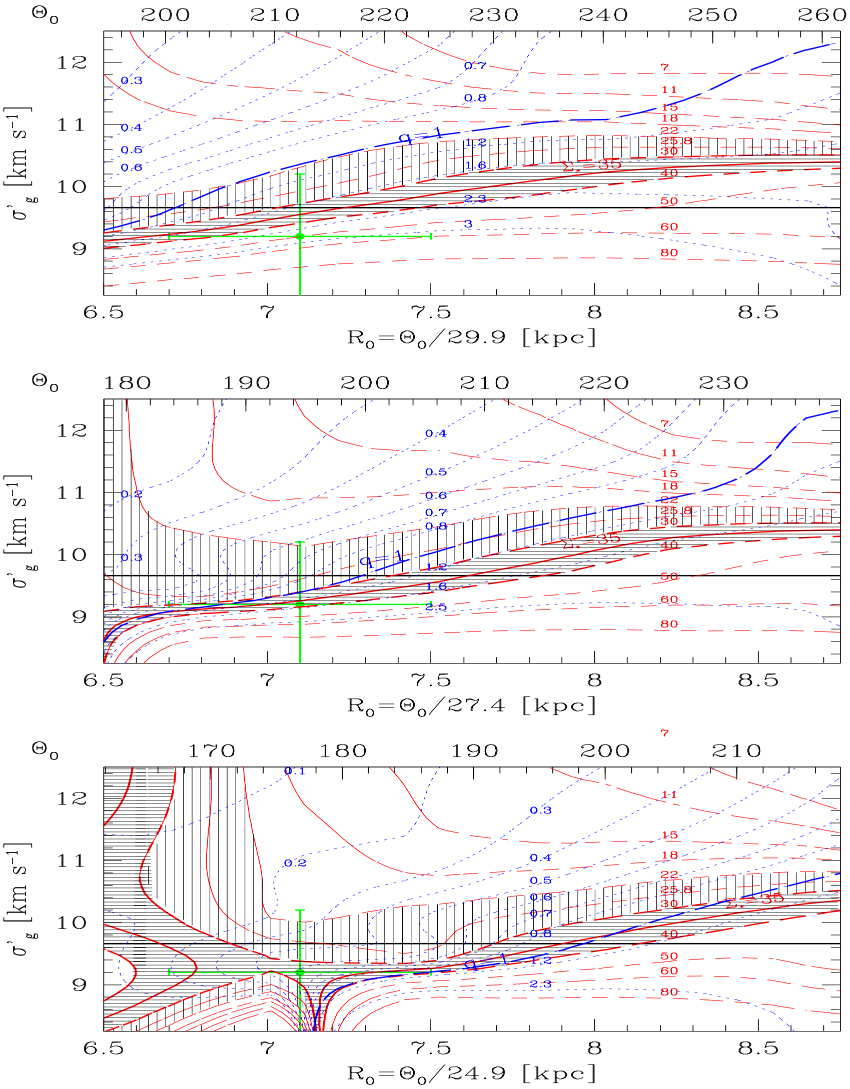

Figure 3. In this figure we present the interrelations between the adopted value of the gaseous velocity dispersion ($\sigma_g{}'$) and the Galactic constants. The line coding is the same as in Figs. 2. This figure was generated by extracting the halo flattening and Σ_* values along the lines $\Theta_0/R_0 = 24.9, 27.4$, and 29.9 (from top to bottom), for several values of the effective gaseous velocity dispersion. The fat cross represents our best estimate for the Galactic constants [$R_0 = 7.1 \pm 0.4$ kpc, $\Theta_0 = 184 \pm 8$ km s^{-1}, (Olling & Merrifield 1997a,1998b)], and the gaseous velocity dispersion [$\sigma_g = 9.2 \pm 1$ km s^{-1}, (Malhotra 1995)]. The thick horizontal line represents our theoretical expectation as to the maximum value of σ'_g (eqn. 24). Large effective velocity dispersions require flattened halos so that the model gas layer widths are as thin as observed. Round, and even prolate, halos are found for small $\sigma_g{}'$ values. In the shaded region of parameter space, the mass of the stellar disk is as measured by KG89 (horizontal dark shading) and GBF97 (vertical light shading).

columndensity and the halo's oblateness severely restrict the allowed range for σ'_g, in particular for $R_0 \geq 7$ kpc.

More specific results follow if we are willing to make more restrictive assumptions. For example, if we assume that $(R_0,\sigma'_g) = (7.2,9.2)$, we find $q \gtrsim 1.1\,(\Omega = 29.9)$, $q \gtrsim 0.6\,(\Omega = 27.4)$, and $q \gtrsim 0.2\,(\Omega = 24.9)$, where these low q values occur at the edge of parameter space where $R_0 \lesssim 6.9$ kpc. Inspecting figure 3, we notice that the $q = 1$ line and the stellar density contours are inclined with respect to each other. Assuming a lower limit for Σ_* and an oblate halo, it is possible to determine an upper limit to Θ_0 for each value of Ω. With $\Sigma_* \geq 30\ M_\odot\,\mathrm{pc}^{-2}$, we find $\Theta_0(q \leq 1) \sim 190-(\Omega-30)+0.6\times(\Omega-30)^2$. Decreasing the lower bound of Σ_* to the value suggested by Gould, Bahcall & Flynn (1997) increases the upper bound to Θ_0 by about 20 km s^{-1}.

Alternatively, when choosing particular values for the Galactic constants, simple relations between the remaining three parameters of the mass model follow. For example, taking the IAU-recommended values for R_0 and Θ_0 (8.5 kpc, and 220 km s^{-1}) we find $q \sim 0.62 - 0.31(\sigma'_g - 11.9) + 0.11(\sigma'_g - 11.9)^2$ and $\Sigma_* \sim 16 - 17(\sigma'_g - 11.1) + 4.8(\sigma'_g - 11.1)^2$.

5 SUMMARY AND CONCLUSIONS

In Paper I we showed that the constraints on the dark matter density in the Solar neighbourhood and the outer Galaxy place tight limits on the choice of the Galactic constants, the mass of the stellar disk, and the dark halo's flattening. In this paper we present the analytical tools that allow for an efficient search through parameter space. Employing these tools, we extend the analysis by investigating the effects of the ill-determined contribution of non-thermal pressure support on the H I flaring, and the consequences for the inferred R_0, Θ_0, Σ_*, and q values. The strongest constraints available are the observed Θ_0/R_0 ratio, the mass of the stellar disk and the fact that the dark halo is almost certainly oblate. Taken together, these constraints rule out substantial contributions to the support of the H I layer beyond the optical disk by cosmic ray pressure or magnetic fields for $R_0 \gtrsim 7$ kpc, in agreement with theoretical predictions [eqn. (24)]. We find that the Milky Way's dark matter halo is close to spherical for all but the smallest values of R_0 or Θ_0. A dark matter halo as flattened as $q = 0.2$ is only possible if our distance to the Galactic centre is smaller than about 6.8 kpc.

It is possible to construct a self-consistent oblate model of the Galaxy with $R_0 = 8.5$ kpc and $\Theta_0 = 220$ km s^{-1}, but only if the local stellar columndensity is less than about 22 $M_\odot$ pc^{-2}, *and* $\sigma'_g \gtrsim 10.8$ km s^{-1}.

The existence of the "vertical disk-halo conspiracy", described in Appendix A, means that stellar kinematical data above about 800 pc are required in order to distinguish between the different possible vertical density profiles. Kuijken & Gilmore's (1991) determination of the columndensity of matter within 1.1 kpc of the plane (71 $\pm$ 6 $M_\odot$ pc^{-2}) is robust and valid over a wide range of Galactic constants and disk scale-lengths. For the stellar contribution to this total mass we suggest a *consensus* average of $\Sigma_* = 35 \pm 10$ $M_\odot$ pc^{-2}.

If $R_0 \gtrsim 7$ kpc, then the dark halo of the Milky Way is fairly close to spherical, independent of the amount of non-thermal pressure support. Such a round halo argues against dissipational baryons as a viable dark matter candidate. Further, since all other baryonic dark matter candidates have already been observationally excluded (Hegyi & Olive 1986), we must conclude that the dark matter halo of the Milky Way is most likely made up of something altogether more exotic (MACHOs, neutrinos, axions, neutralinos ...). Even in the Solar neighborhood, there are non-negligible quantities of this material: our proposed dark halo models imply that it amounts to some 0.42 GeV/c^2 per cubic centimetre or (11 $\pm$ 5) m$M_\odot$ pc^{-3}. The direct detection of this material remains a challenge for experimental physicists.

Our model imposes strong correlations between the parameters of the mass model. We presented several examples in the previous section. Since we make strong predictions as to the values of R_0, Θ_0, Σ_*, q and σ'_g (Figs. 2 and 3), our models can be subjected to experimental verification. For example, all parameters but σ'_g could be determined using astrometric data from future space missions such as NASA's SIM and ESA's GAIA. Such high precision data are ideally suited to support, or falsify, the models we propose here. Whatever the outcome, we will learn a great deal more about the structure and dynamics of the Milky Way galaxy.

ACKNOWLEDGMENTS

We thank Andy Newsam, Irini Sakelliou, Konrad Kuijken, Marc Kamionkowski, Jacqueline van Gorkom, Chris McKee, and James Binney for useful discussions. RPO thanks Columbia University's Astronomy department for its hospitality. This research has made use of NASA's Astrophysics Data System Abstract Service.

REFERENCES

Backer D.C., 1996, in Blitz L., Teuben P., eds, Unsolved Problems of the Milky Way
Bahcall J.N., Flynn C., Gould A., 1992, ApJ, 389, 234
Bahcall J.N., 1984a, ApJ, 276, 156
Bahcall J.N., 1984b, ApJ, 276, 169
Becquaert J.F., Combes F., Viallefond F. 1997, A&A, 325, 41
Begeman K., 1989, A&A, 223, 47
Begeman K., 1987, Ph. D. Thesis, University of Groningen
Bergstrom L., Ullio P., Buckley J.H., 1997, astro-ph/9712318
Bicay M.D. & Helou G., 1990, ApJ, 362, 59
Bienaymé O., Robin A.C. & Crézé M., 1987, A&A, 180, 94
Blitz L., Spergel D.N., 1991, ApJ, 370, 205
Bottema R., 1993, A&A, 275, 16
Brand J., Blitz L., 1993, A&A, 275, 67
Bronfman L., Cohen R.S., Alvarez H., May J. & Thaddeus P., 1988, ApJ, 324, 248
Burton W.B., 1988, in Verschuur G.L., Kellermann K.I., eds, Galactic and Extragalactic Radio Astronomy, p. 295
Bosma A., 1981, AJ, 86, 1825
Broeils A., 1992, Ph. D. Thesis, University of Groningen
Casertano S., van Gorkom J.H., 1991, AJ, 101, 1231
Côté S., 1995, Ph.D. Thesis, Mt. Stromlo and Siding Sprint Observatories Australian National University
Crézé M., Chereul E., Bienaymé O., Pichon C., 1998, A&A, 329, 920
Crézé M., Robin A.C. & Bienaymé O., 1989, A&A, 211, 1
Dehnen W., Binney J., 1998, MNRAS, 294, 429
Dickey J.M., Hanson M.M. & Helou G., 1990, ApJ, 352, 522
Ellis R.S., Axon D.j., 1978, Astrophysics and Space Science, 54, 425
Flynn C., Fuchs B., 1994, MNRAS, 270, 471
Freudenreich, H.T., 1998, ApJ, 492, 495
Freudenreich, H.T., 1996, ApJ, 468, 663
Gates E.I., Gyuk G., Turner M.S., 1995, PhRvL, 74, 3724
Gould A., Bahcall J.N., Flynn C. 1997, ApJ, (GBF97)
Hegyi D. & Olive K.A., 1986, ApJ, 303, 56
Kamphuis J., 1993, Ph.D. Thesis, University of Groningen
Kent S.M., 1992, ApJ, 387, 181
Kent S.M., 1987, AJ, 93, 816
Kent S.M., Dame T.M. & Fazio G., 1991, ApJ, 378, 131
Kerr F.J., Lynden-Bell D., 1986, MNRAS, 221, 1023

Kim J., Hong S.S., Ryu D., Jones T.W., 1998, ApJ, 506L, 139
Kuijken K. & Gilmore G., 1991, ApJ, 367, L9 (KG91)
Kuijken K. & Gilmore G., 1989b, MNRAS, 239, 605 (KG89)
Kuijken K. & Gilmore G., 1989a, MNRAS, 239, 571
Kulkarni S.R., & Heiles C., 1988, in Hollenbach D.J., Thronson H.A. Jt., Interstellar Processes, p. 87
Lake G., Feinswog L., 1989, AJ, 98, 166
Malhotra S., 1995, ApJ, 448, 138
Merrifield M.R., 1992, AJ, 103, 1552
McGaugh S.S., de Blok W.J.G., 1998, ApJ, accepted for publication, astro-ph/9801123
Navarro J., Frenk C.S., White S.D.M., 1996, ApJ, 462, 563
Olive K.A., Steigman G., 1995, ApJS, 97, 490
Olling R.P., Merrifield M.R., 1999, MNRAS, accepted for publication (Paper I)
Olling R.P., Merrifield M.R., 1999, MNRAS, accepted for publication (Paper I)
Olling R.P., Merrifield M.R., 1998, MNRAS, 297, 943
Olling R.P., Merrifield M.R., 1997a, in the proceedings of the Santa Cruz' "Galactic Halos" workshop, astro-ph/9711157
Olling R.P., Merrifield M.R., 1997b, in the proceedings of the Santa Cruz' "Galactic Halos" workshop, astro-ph/9710224
Olling R.P., 1997c, in Klapdor-Kleingrothaus H.V., Ramachers Y., eds, "Aspects of Dark Matter in Astro- and Particle Physics", p. 44, World Scientific, *astro-ph/9612018*
Olling R.P., 1996a, AJ, 112, 481-490
Olling R.P., 1996b, AJ, 112, 457-480
Olling R.P., 1995, AJ, 110, 591

Parker E.N., 1966, ApJ, 145, 811
Persic M., Salucci P., Stel F., 1996, MNRAS, 281, 27
Pfenniger D., Combes F., & Martinet L., 1994, A&A, 285, 79
Pont F., Queloz D., Bratchi P., Mayor M., 1997, A&A, 318, 416
Reid M.J., Readhead A.C.S., Vermeulen R.C., Treuhaft R.N., 1999, astro-ph/9905075
Reid M.J., 1993, ARA&A, 31, 345
Robin A.C., Crézé M. & Mohan V., 1992, ApJ, 400, L25
Rubin V.C., Ford W.K., Thonnard N., 1980, ApJ, 238, 471
Rupen M.P., 1991, Ph. D. Thesis, Princeton University
Sackett P.D., 1997, ApJ, 483, 103
Sackett P.D., Sparke L.S., 1990, ApJ, 361, 408
Sancisi R., Allen R.J., 1979, A&A, 74, 73
Sciama D., 1990, MNRAS, 244, 1
Sicking F., 1997, Ph.D. Thesis, University of Groningen
Spitzer L., 1978, Physical Processes in the Interstellar Medium, John Wiley & sons (New York)
Albada T.S. van & Sancisi R., 1986, Phil. Trans. R. Soc. Lond. A., 320, 447
van Albada T.S., Bahcall J.N., Begeman K., Sancisi R., 1985, ApJ, 295, 305
van der Kruit P.C., 1988, A&A, 192, 117
van der Kruit P.C., 1981, A&A, 99, 298
Shostak S., van der Kruit P.C., 1984, A&A, 132, 20
Wielen R. 1974, Highlights of Astronomy, 3, 395

APPENDIX A: MORE ON THE VERTICAL DISK-HALO CONSPIRACY

In section 3.1 we reviewed the stellar kinematical route to determine the local stellar columndensity. In this appendix we try to emulate and check this method in some detail. In order to do so we calculate the exact vertical force law $K_{\rm z,exact}$ for a limited number of Galaxy models listed in Table 2 using the global approach (§ 3.3; Olling 1995). We also compute an approximation to $K_{\rm z,exact}$ from the local mass distribution (§ 3.3; Olling 1995), which follows from an integration of the poisson equation:

$$K_{\rm z,local}(z) \quad = \quad -4\pi G \int_0^z dz' \left[\rho_m(z') + \rho_{rot}\right] \, , \qquad \text{(A1)}$$

with ρ_m the matter density, $\rho_{rot}(\equiv \frac{-2}{4\pi G}\frac{V_{rot}}{R}\frac{dV_{rot}}{dR})$ a pseudo density which arises from gradients in the rotation curve, and $K_{\rm z}$ the vertical force per unit mass.

In figure A1 we present true vertical force (filled circles) and the local approximation (open circles) for one particular combination of parameters which lie close to the best estimates for the Milky Way (Kuijken & Gilmore 1989, 1991; Olling & Merrifield 1998). We see that in the Solar neighborhood and close to the plane, the local approximation is reasonably accurate‖‖ and can be used as an approximation to the true vertical force law. Significant deviations from the true $K_{\rm z}$ only occur above approximately 800 pc. We also include the observationally determined $K_{\rm z}$ [crosses with error bars; KG89's equation (1) with D=250 pc].

Now we investigate the possibility that the actual dark matter density law differs from the distribution in our models [eqn. (1)]. Choosing a different DM distribution while keeping the observed $K_{\rm z}$ fixed requires a different luminous mass distribution. As a simple test case, we plot a model where the DM density is multiplied by 1.92 (labeled "dGR+Hx1.92" in Fig. A1). In this case, we have to decrease the stellar columndensity to the GBF97 value (25.8 $M_\odot\,{\rm pc}^{-2}$) in order to keep $K_{\rm z}$ approximately unchanged. Next we consider DM distributions inspired by Bahcall's "P" models (1984b), where the DM density is assumed to be a linear combination of the known components:

$$\rho_{err} \;=\; X_d \times \rho_d + X_g \times \rho_g + X_h \times \rho_h + X_{rot} \times \rho_{rot} \, , \quad \text{(A2)}$$

where the subscripts d, g, h denote the disk, gas, and halo components, respectively. Using this formalism, we can calculate the columndensities of all components (ISM, stars, DM and $\Sigma_{tot}^{1.1}$) which arise from a particular choice of the X_i-values. From such an erroneous density distributions (ρ_{err}) we determine the erroneous vertical force ($K_{z,err}$) using equation (A1). We present the $K_{z,true}/K_{z,err}$ ratio, averaged in several z-height ranges, in Table A1 (columns 5-7). In this table we also list the X_i, Σ_* and $\Sigma_{tot}^{1.1}$ values for some models. In addition to the P-models, we also evaluate models in which we keep the ISM and ρ_{rot} contributions fixed while varying the stellar and dark matter densities such that the

‖‖ For the ensemble of models for which the parameters differ by $\leq$ 1-σ from the model presented here, the approximations based on equation (A1) reproduce the true $K_{\rm z}$ typically to within **7%**: sometimes models that include the rotation curve gradient term perform best, sometimes not. The same is true for the models listed in Table 2 with other Galactic constants than those presented in figure A1.

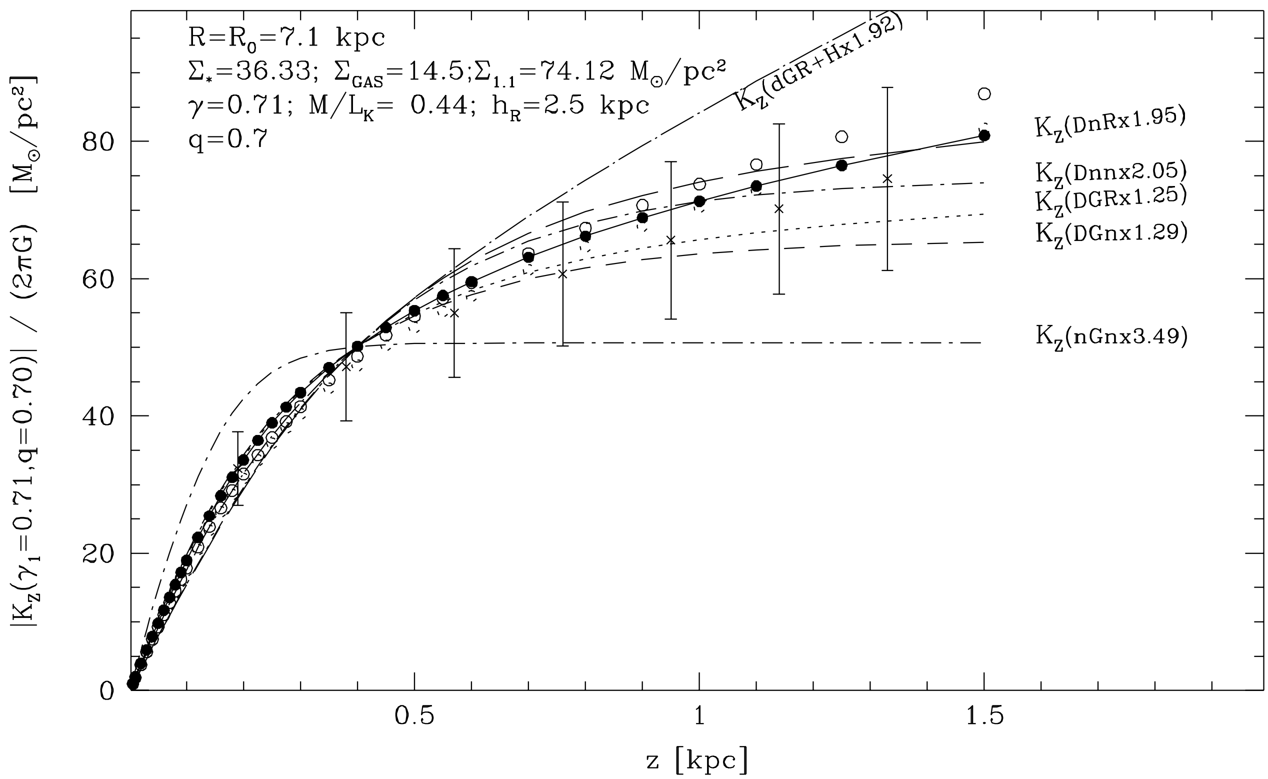

Figure A1. We present the exact vertical force (filled circles) at Galactocentric distance R_0 for a model that almost reproduces the values for Σ_* and $\Sigma_{tot}^{1.1}$ proposed by Kuijken & Gilmore (1989, 1991). The local approximation to the exact force law that uses the slope of the rotation curve (open circles) or assumes a flat rotation curve (dashed open circles) are also indicated. Some other models in which the DM is distributed like various superpositions of the known components are also plotted: 1) $\rho_{DM} = 1.29 \times (\rho_* + \rho_g)$ (labeled "DGnx1.29'); 2) $\rho_{DM} = 1.25 \times (\rho_* + \rho_g + \rho_{rot})$ ("DGRx1.25"); 3) $\rho_{DM} = 2.05 \times \rho_*$ ("Dnnx2.05"); 4) $\rho_{DM} = 1.95 \times (\rho_* + \rho_{rot})$ ("DnRx1.95"); 5) $\rho_{DM} = 3.49 \times \rho_g$ ("nGnx3.49"). For the curve labeled "dGR+Hx1.92" we used a smaller columndensity of stars 25.8 $M_\odot\,\mathrm{pc}^{-2}$ (Gould, Bahcall & Flynn 1997), and multiplied the halo contribution by 1.92. Most of the models have very similar force laws in the region close to the plane (see also Table A1). We also include KG89's vertical force law and the errors thereupon (crosses with error bars).

force at 400 pc above the plane equals the true value. From table A1 we see that it is possible to decrease Σ_* by more than an order of magnitude and simultaneously increase X_h without altering $K_z(|z| \leq 800\mathrm{pc})$ substantially. It seems that the vertical distribution of dark and stellar matter conspire in such a way that their relative contributions can not be easily separated. Thus, this "vertical disk-halo conspiracy" is much like the classical disk-halo conspiracy which arises in considerations of the radial distribution of luminous and dark luminous matter derived from galaxy rotation curves.

From the data presented in Table A1 it is clear that, without additional assumptions, stellar kinematical data extending to a few hundred parsec are not sufficient to determine the mass of the stellar disk. However, $\Sigma_{tot}^{1.1}$ is much better determined (rightmost column of Table A1), in agreement with Kuijken & Gilmore (1991). In order to discriminate between models, it is essential to incorporate a rotation curve constraint to limit the possible DM densities. Kuijken & Gilmore (1989) used such a constraint explicitly, while Bahcall (1984b) and Flynn & Fuchs (1994) used "reasonable" values for the density of non-disk-like dark matter to rule out extreme values for the mass of the stellar disk. Furthermore, if data at larger z are considered, the differences between the force laws shown in figure A1 start to become apparent and can be used to limit the range in Σ_* (Flynn & Fuchs 1994).

Although the the model parameters we have used to construct Figure A1 and Table A1 lie at the extreme end of the models investigated by Kuijken & Gilmore, we find that other models, within the 1-2σ range of Θ_0/R_0 , h_d, Σ_*, and $\Sigma_{tot}^{1.1}$, yield similar results. Thus, mass models for the Milky Way *have* to conform to the constraint $\Sigma_{tot}^{1.1}$= (71 ± 6) $M_\odot\,\mathrm{pc}^{-2}$. To summarize the above, in order to determine the stellar columndensity from stellar kinematics, the existence of a vertical disk-halo conspiracy requires that in order to make a kinematical determination of Σ_*, one *has* to include rotation curve constraints and/or sample the region above 800 pc.

Table A1. The accuracy to which various erroneous density distributions can reproduce the true vertical force. The first four columns describe which $\rho(z)$ was used [cf. eqn. (A2)]. The next three columns indicate the average ratio of $K_{z,\rm true}/K_{z,\rm err}$ over the vertical ranges indicated [0 - 0.4 kpc (Z1), 0.4 - 0.8 kpc (Z2), and 0.8 - 1.2 kpc (Z3)]. The typical variation within these radial ranges is a few %, except for the gas-only case where it can be up to 35%. We also indicate the model values for Σ_* and $\Sigma_{tot}^{1.1}$, in units of $M_\odot\,{\rm pc}^{-2}$. The last two lines give the average and standard deviations of the lines above (excluding the gas-only model).

X_d	X_g	X_{rot}	X_h	Z1	Z2	Z3	Σ_*	$\Sigma_{tot}^{1.1}$
1.25	1.25	1.25	0.00	1.03	0.99	0.93	45.4	63.6
1.29	1.29	0.00	0.00	0.95	1.04	1.17	46.9	65.6
2.05	0.00	0.00	0.00	0.85	1.03	1.01	74.5	74.5
1.95	0.00	1.95	0.00	0.85	1.03	1.04	70.8	70.8
0.00	3.49	0.00	0.00	1.35	0.90	0.72	0.0	50.6
1.40	1.00	1.00	0.03	1.03	0.99	0.93	50.9	66.1
1.25	1.00	1.00	0.46	1.03	0.99	0.93	45.4	70.6
1.00	1.00	1.00	1.17	0.97	1.02	1.08	36.3	78.1
0.74	1.00	1.00	1.92	0.95	1.04	1.17	26.9	86.1
0.50	1.00	1.00	2.59	0.93	1.06	1.24	18.2	92.9
0.25	1.00	1.00	3.30	0.92	1.08	1.33	9.1	100.4
0.12	1.00	1.00	3.67	0.91	1.09	1.37	4.4	104.3
							39±	77±
							58%	21%

APPENDIX B: STELLAR KINEMATICS AND THE RELATION BETWEEN THE MODEL'S PARAMETERS

In section 3.2 we described how the observationally determined $\Sigma_{tot}^{1.1}$-value imposes correlations between luminous and dark matter in the Solar neighbourhood. The existence of the vertical disk-halo conspiracy shows that it is difficult to exactly determine Σ_* kinematically. In this section we present some specific examples to illustrate what we can learn about the structure of the Milky Way by treating Σ_* as a parameter which is only constrained by $\Sigma_{tot}^{1.1}$ [cf. eqn (5)].

At the Solar circle, and for $z = 1.1$ kpc, equation (4) can be rearranged to read:

$$\frac{\Sigma_h^{1.1}(q)}{\Sigma_h^{1.1}(1)} \approx 1.1R_0 + R_0\,(0.9 - R_0)\,q \qquad q \lesssim 0.15 \qquad \text{(B1)}$$

$$\approx \quad q^{-13/20}\,, \qquad q \gtrsim 0.15 \qquad \text{(B2)}$$

where the core radius has been set to R_0. In this appendix we use –for the sake of convenience– the symbol q for the halo flattening derived from the local stellar kinematics constraint, and $q_{\rm H\,I}$ for the halo's shape derived from the H I flaring. Taking the fiducial values for $\Sigma_{tot}^{1.1}$, Σ_*, and Σ_g to be 71, 35, and 14.5 $M_\odot\,{\rm pc}^{-2}$, respectively, and employing equation (5) we determine the fiducial value for $\Sigma_h^{1.1}$ to be 21.5 $M_\odot\,{\rm pc}^{-2}$. Further, defining $\Sigma_* = 35 + \delta\Sigma_*$, use the fiducial columndensities defined above, and apply equations (B1) and (B2), we can relate the required halo flattening to $\delta\Sigma_*$:

$$q \approx \frac{21.5 - R_0\,\Sigma_h^{1.1}(1) - \delta\Sigma_*}{0.9R_0^2\Sigma_h^{1.1}(1)} \qquad \text{(B3)}$$

$$\approx \left(\frac{\Sigma_h^{1.1}(1)}{21.5}\right)^{20/13}\left[1 + \left(\frac{20/13}{21.5}\right)\delta\Sigma_*\right] \qquad \text{(B4)}$$

for the same q-ranges as in Eqns. (B1) and (B2). Since $\Sigma_h^{1.1}(q=1)$ depends on Θ_0 [eqn. (4)], the solutions of equations (B3) and (B4) depend on R_0, Θ_0, and $\delta\Sigma_*$. We use our mass models to determine $\Sigma_h^{1.1}(q=1; R_0, \Theta_0)$ and rewrite equations (B3) and (B4) for a few interesting cases. For $\delta\Sigma_* = 0$ we find:

$$q \approx 0.07 \pm 0.05 \qquad (\Theta_0 = 165) \qquad \text{(B5)}$$

$$q \approx 0.4 - 0.1(R_0 - 7.1) \pm 0.1 \qquad (\Theta_0 = 175) \qquad \text{(B6)}$$

$$q \approx 0.8 - 0.2(R_0 - 7.1) \pm 0.2 \qquad (\Theta_0 = 185) \qquad \text{(B7)}$$

Thus, lower rotation speeds and larger R_0's require more highly flattened halos. Furthermore, for any fixed value of R_0, the *slope* of the $q - \delta\Sigma_*$ relation depends strongly upon Θ_0. For example, with R_0=7.1 kpc we find:

$$q \approx 0.069 + 0.005\,\delta\Sigma_* \qquad (\Theta_0 = 165) \qquad \text{(B8)}$$

$$q \approx 0.400 + 0.030\,\delta\Sigma_* \qquad (\Theta_0 = 175) \qquad \text{(B9)}$$

$$q \approx 0.800 + 0.060\,\delta\Sigma_* \qquad (\Theta_0 = 185) \qquad \text{(B10)}$$

Equations (B5) through (B10) clearly show that small values of the Galactic rotation speed imply a highly flattened dark matter halo, whatever our distance to the Galactic centre, and whatever the mass of the stellar disk. We also see that the last three relations constrain Σ_* rather tightly: for models with $\Theta_0 \lesssim 185$ km s^{-1}, an increase in the stellar columndensity of $\sim$10 $M_\odot\,{\rm pc}^{-2}$ covers the whole allowed range for q. Note that all these constraints are completely independent of the H I flaring.

In section 4.2 and figure 2 we have see the stellar kinematics and H I flaring constraints provide mutually exclusive constraints on Σ_* and q if both the rotation speed and the effective velocity dispersion are small. This can be understood as follows: equations (B5)-(B10) show that the $\Sigma_{tot}^{1.1}$ constraint implies small q-values for low Θ_0's. Likewise, the H I flaring constraint yields small q's for small Θ_0's, but only if the velocity dispersion does not decrease by too much [cf. eqn. (15)]. Furthermore, because the slope of the $q(\Sigma_*)$ relation becomes shallower with decreasing Θ_0, the allowed range for $q_{1.1}$ decreases with Θ_0 [cf. eqn. (B5) and (B8)]. Thus, extreme values for Σ_* are required to match q with $q_{\rm H\,I}$. Obviously, if the required stellar column exceeds $\Sigma_{tot}^{1.1}$, no self-consistent model is possible for that particular combination of Galactic constants and gaseous velocity dispersion. In these circumstances it is possible that our procedure to determine Σ_* and q arrives at extreme values for Σ_* and q, or sometimes even negative values.

APPENDIX C: THE ISM OF THE MILKY WAY TABULATED

In this appendix we present a tabulated version of the radial variation of the atomic and molecular hydrogen, as well as their widths. We present these data in a manner which is *independent* of the values of the Galactic constants as well as the shape of the rotation curve. The H I columndensity at the Solar position includes 1.4 $M_\odot\,\mathrm{pc}^{-2}$ of ionized hydrogen. No ionized hydrogen is included at any other radius. The columndensities listed do not include the contribution due to Helium. In our model calculations of the potential we increase the listed columndensities to include 23.8% Helium. We have brought the data from the sources listed in section 2.1 onto a common distance scale defined by Merrifield's (1992) determination of the $W(R/R_0) = v_{rad}/(\sin l \cos b)$ curve. Here v_{rad} and l and b are the radial velocity and the Galactic coordinates, respectively. In practice this rescaling works as follows: 1) from the rotation curve $[\Theta'(R')]$ in the original reference, determine R'/R'_0 and $W'(R'/R'_0) \equiv R'_0[\Theta'(R')/R' - \Theta'_0/R'_0]$ [the primed quantities refer to the values assumed in the reference], 2) for each property X' (gas layer width, surface or volume density), determine $X'(W')$ from $X'(R')$ and $W'(R')$, 3) find Merrifield's R/R_0 values for which $W = W'$, 4) X' re-gridded onto Merrifield's distance scale is now given by $X(R/R_0)$.

Table C1. The surface density and thickness of the atomic and molecular hydrogen components in the Milky Way as a function of Galactocentric radius. The widths are expressed in units of R_0, the columndensities in $M_\odot\,\mathrm{pc}^{-2}$. For $R > R_0$, the widths of the H I layer is the average of several works, see Paper I for details. Some entries have been left blank: we were unable to derive reliable widths at these radii. The columndensities at these radii are from Wouterloot *et al.* (1990).

R $[R_0]$	$\Sigma_{\mathrm{H\,I}}$ $M_\odot\,\mathrm{pc}^{-2}$	$\Sigma_{\mathrm{H_2}}$ $M_\odot\,\mathrm{pc}^{-2}$	$\mathrm{FWHM}_{\mathrm{H\,I}}$ $[R_0]$	$\mathrm{err}_{\mathrm{H\,I}}$ $[R_0]$	$\mathrm{FWHM}_{\mathrm{H_2}}$ $[R_0]$
0.218	0.59	1.08	0.0330	0.0014	0.0151
0.276	1.04	1.54	0.0320	0.0031	0.0158
0.309	1.23	1.47	0.0323	0.0017	0.0134
0.343	1.30	1.67	0.0306	0.0014	0.0119
0.376	1.29	2.67	0.0294	0.0008	0.0131
0.409	1.31	4.29	0.0268	0.0045	0.0140
0.440	1.41	4.91	0.0290	0.0031	0.0142
0.467	1.59	5.02	0.0313	0.0028	0.0143
0.499	1.85	5.57	0.0278	0.0011	0.0153
0.530	2.10	6.23	0.0240	0.0017	0.0165
0.559	2.30	5.87	0.0301	0.0014	0.0168
0.586	2.48	5.48	0.0346	0.0014	0.0163
0.612	2.90	5.18	0.0344	0.0023	0.0152
0.641	3.72	4.62	0.0415	0.0034	0.0139
0.668	4.36	3.94	0.0504	0.0017	0.0129
0.692	4.24	3.73	0.0525	0.0014	0.0120
0.717	3.60	3.97	0.0447	0.0031	0.0115
0.742	3.17	4.27	0.0452	0.0039	0.0122
0.764	3.23	4.33	0.0485	0.0130	0.0136
0.786	3.68	4.09	0.0495	0.0101	0.0152
0.806	4.22	3.60	0.0565	0.0039	0.0161
0.828	4.72	2.95	0.0530	0.0048	0.0159
0.848	4.90	2.44	0.0570	0.0034	0.0144
0.865	4.80	2.06	0.0572	0.0011	0.0134
0.882	4.52	1.70	0.0509	0.0014	0.0136
0.897	4.41	1.45	0.0525	0.0020	0.0146
0.913	4.75	1.30	0.0523	0.0036	0.0158
0.926	5.39	1.26	0.0652	0.0017	0.0167
0.938	6.13	1.29	0.0730	0.0020	0.0174
1.000	9.25	1.80	0.0577	0.0042	0.0199
1.058	8.57	1.80			
1.089	7.77	1.28	0.0611	0.0044	0.0238
1.193	6.09	0.44			
1.332	6.56	1.62	0.0734	0.0061	0.0385
1.457	7.45	1.47			
1.586	7.62	1.10	0.0801	0.0062	0.0458
1.721	6.02	0.54			
1.848	5.30	0.37	0.1108	0.0099	0.0742
1.995	4.36	0.20			
2.101	3.41	0.11	0.1391	0.0115	0.0767
2.177	3.31	0.14			
2.262	2.84	0.12			
2.355	2.36	0.09	0.1666	0.0143	
2.443	2.01	0.05			
2.532	1.66	0.01			